Nutrients in Water Masses in the Atlantic Sector of the Arctic Ocean: Temporal Trends, Mixing and Links With Primary Production

Pedro Duarte[1] , Amelie Meyer[2,3] , and Sebastien Moreau[1]

[1]Norwegian Polar Institute, Fram Centre, Tromsø, Norway, [2]Institute for Marine and Antarctic Studies, University of Tasmania, Hobart, TAS, Australia, [3]ARC Centre of Excellence for Climate Extremes, University of Tasmania, Hobart, TAS, Australia

Abstract There is strong evidence of an increase in primary production (PP) in the Arctic Ocean (AO) over the last two decades. Further increases will depend on the interplay between decreasing light limitation for primary producers, as the sea ice extent and thickness decrease, and the availability of nutrients, which is controlled by, but not limited to, inputs from the Atlantic and the Pacific Oceans. While these inputs are the major nutrient sources to the AO, ocean vertical mixing is required to bring the nutrients into the photic zone. We analyze data collected in the Western Eurasian Basin (WEB) between 1980 and 2016 and characterize the nutrient climatology of the various water masses. We conclude that there were no significant trends in the concentrations of the two macronutrients that typically limit PP in the AO (nitrate and silicic acid, in the case of diatoms), except a decreasing trend for silicic acid in Polar Surface Water (PSW), which is consistent with the reported increase in PP in the AO. We suggest that the Whalers Bay polynya, located in the northwestern corner of Svalbard, may act as a mixing hotspot, creating patches of nutrient replenished PSW. These patches may then be advected to higher latitudes under the ice pack, later boosting PP upon release from light limitation or else, keeping a nutrient reservoir that may be used in a subsequent growth season. It is likely that this remaining nutrient reservoir will decrease as sea ice cover retreats and light limitation alleviates.

Plain Language Summary There is strong evidence of an increase in primary production (PP) in the Arctic Ocean (AO) over the last two decades. This has strong implications for global biogeochemical cycles and on how the AO mitigates the increase in greenhouse gases. However, predicting how much PP will further increase depends on the interplay between decreasing light limitation for primary producers, as the sea ice extent and thickness decrease, and the availability of nutrients, such as nitrate, phosphate, and silicic acid (abbreviated as silica). We analyzed data collected over more than three decades in the Western Eurasian Basin (WEB) of the AO (1980–2016). We conclude that the nutrient concentrations of the various water masses found in this area have not changed significantly, except for the surface water masses, where there is a decreasing trend in silica concentration. This trend is consistent with the reported increase in PP. Our study provides a baseline for the nutrient composition of the water masses found in the WEB to follow their changes in the near future.

1. Introduction

Several empirical and modeling studies show an increase in Arctic Ocean primary production over the last two decades, associated with a reduction in sea-ice cover and increased light availability for phytoplankton and ice algae (e.g., Ardyna & Arrigo, 2020; Arrigo & van Dijken, 2015; Vancoppenolle et al., 2013 and references therein). Empirical evidence of such trends comes mainly from permanently open water areas or areas with seasonal ice cover, such as the Barents Sea, where satellite derived chlorophyll data have been collected for a few decades. Ultimately, primary production will be limited by available nutrients and there seems to be a widespread consensus on the limiting role of nitrate in primary production yields in the Arctic Ocean. Coupled model intercomparison project phase 5 (CMIP5) simulations show a large spread in the degree of nitrate limitation and the main source of this uncertainty is the sea ice zone (Vancoppenolle et al., 2013). Concurrent changes in storm frequency (e.g., Graham et al., 2017, 2019), wind fetch, freshwater flows, stratification, water mass exchanges with lower latitudes (e.g., Ardyna et al., 2014; Randelhoff,
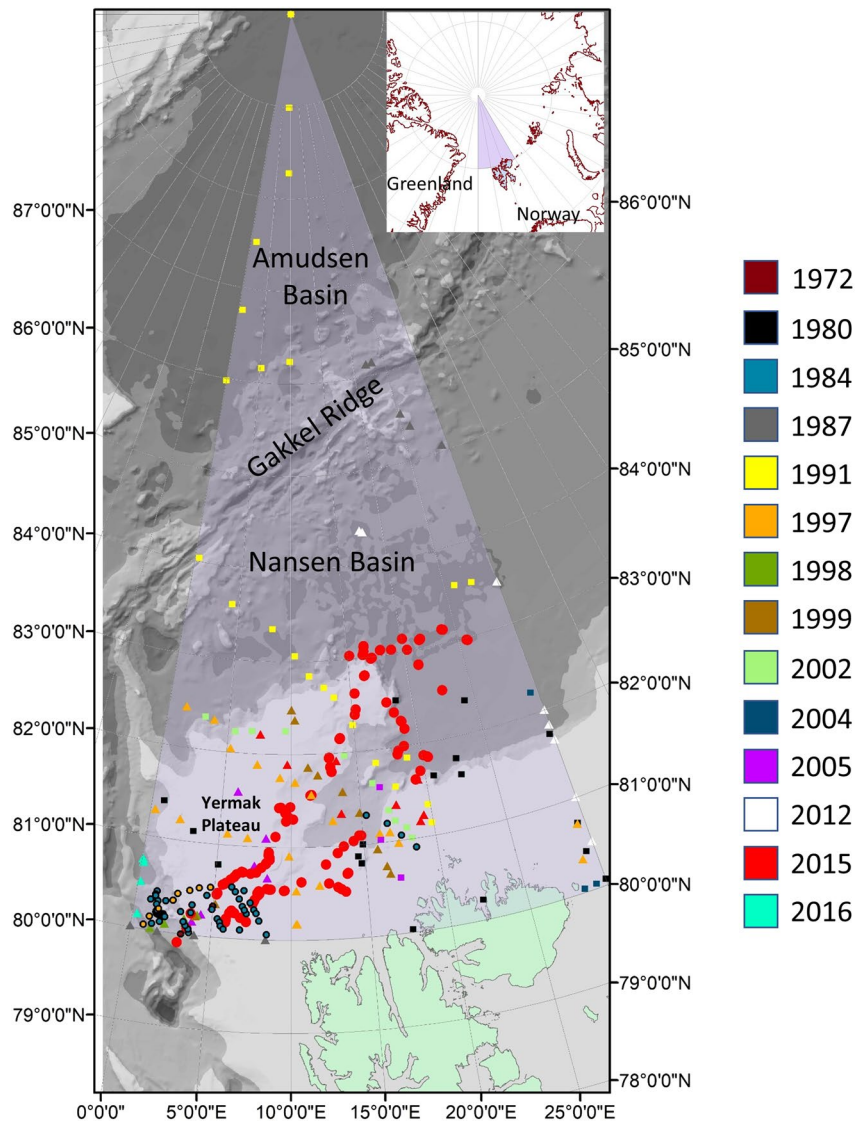
Figure 1. Geographic extent of the study area shown by the transparent polygon, covering the latitude and longitude ranges: 80–90°N and 0–30°E, respectively. The insert in the upper right corner shows the placement of the study area in a wider geographical context. Red circles show the location of nutrient N-ICE2015 sampling sites, obtained from datasets specified in Methodology 2.2. Triangle, squares, and circles with a black outline show the location of nutrient sampling sites in the PANGEA, Carbon in Atlantic Ocean (CARINA) and Codispoti et al. (2013) datasets, respectively (Table 1). Different colors are used for each year as indicated in the legend to the right of the map (see text).

Fer, et al., 2016) and possible changes in the chemical composition of these water masses, with direct and indirect effects on nutrient availability within the photic zone, make it challenging to predict the potential for increase of primary production in the Arctic Ocean.

Pacific water (PW) and Atlantic water (AW) are the two main sources of nutrients in the Arctic Ocean (Torres-Valdés et al., 2013). Polyakov et al. (2020) reported an Arctic-wide decrease in halocline nutrient concentrations, between 1981 and 2017, except in the northern portions of the Makarov and Amundsen Basins and northern Chukchi Sea and Canada Basin. However, their study included a relatively small number of samples from the Eurasian Basin as compared to the Amerasian Basin and only relates to nutrient concentrations in the halocline.

Here we focus on the Western Eurasian Basin (WEB) region (more details are given below in 2.1), which is directly under the influence of the AW inflow through the Fram Strait (Figures 1 and 2). There is evidence of
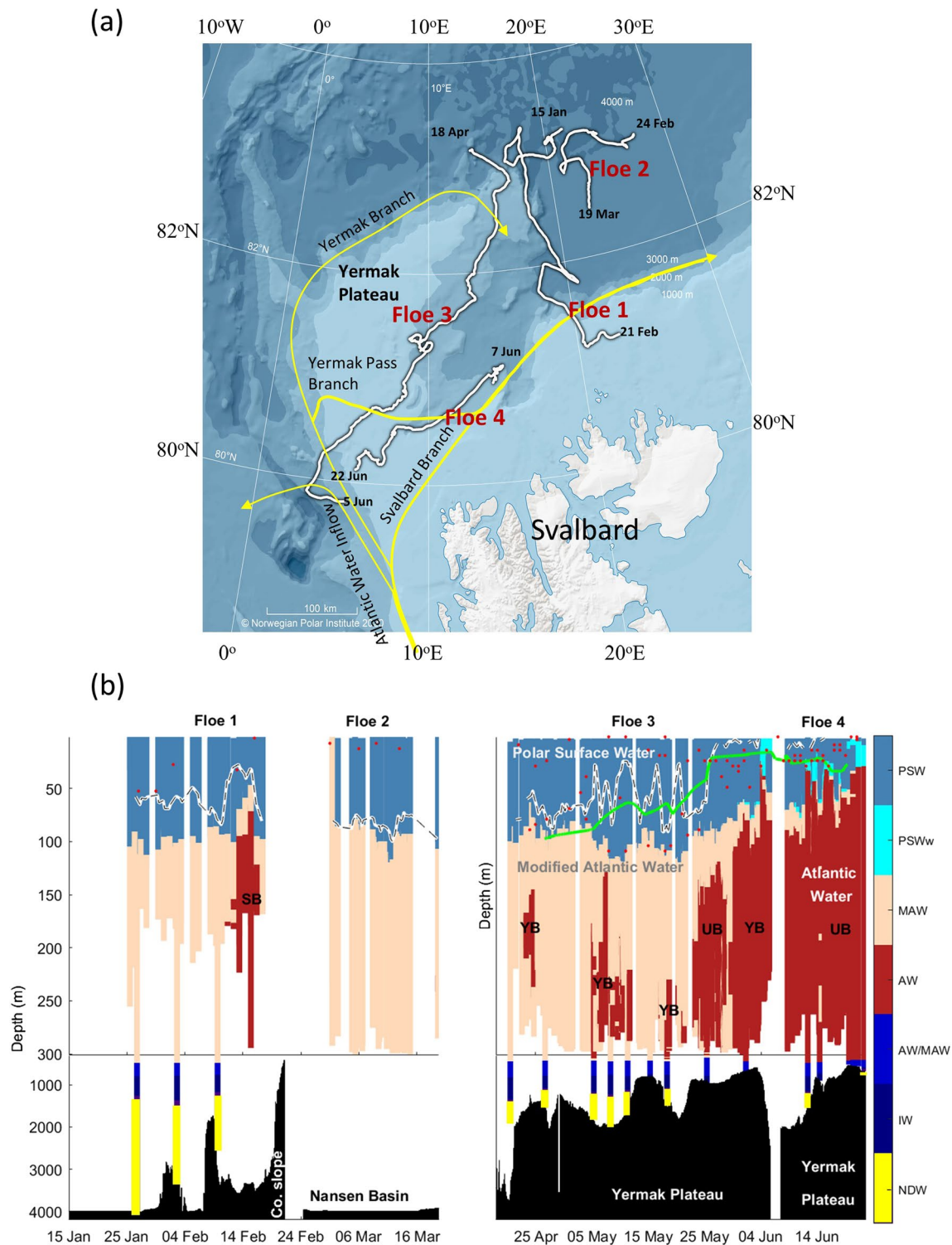
Figure 2.

a significant warming of this inflow during the past ~120 years (Spielhagen et al., 2011), totaling ~2°C since the 1960s (Muilwijk et al., 2018). This is consistent with the positive AW temperature anomalies between 1990 and 2010 of up to 1°C, relative to temperature measurements in the 1970s (Polyakov et al., 2020). These warming trends have caused a weakening of the stratification between the surface water masses and deeper

nutrient rich AW, possibly leading to enhanced nutrient exchanges and primary production increases in surface waters (Nishino et al., 2013; Polyakov et al., 2020).

Our study covers the period 1980–2016 with the following main goals: (a) to investigate temporal trends in nutrient concentrations; (b) to characterize the nutrient climatology of the WEB; and (c) to analyze potential mechanisms of nutrient replenishment that have a profound effect on primary production.

The spatial and temporal sparsity of the available historical data, in particular at intra-annual time scales makes it challenging to identify temporal trends and their causes. We focus our analysis on individual water masses to circumvent this challenge. Our rationale is based on the following: (a) Arctic water masses have been identified based on salinity and temperature ranges (e.g., Rudels et al., 2000); (b) Their relative position in the water column is well known and almost seasonally independent (e.g., Meyer, Sundfjord, et al., 2017); (c) We hypothesize that these water masses should have relatively constrained and distinct nutrient signatures except for those in the photic zone subjected to photosynthesis and intensive nutrient consumption; (d) long-term changes in nutrient contents of the water masses may result from more or less mixing between them, upstream enrichment and biogeochemical trends in for example, primary production, remineralization, denitrification, ammonification and nitrification. Focusing on water masses bypasses confounding changes resulting from trends in physical processes, such as mixing mechanisms, with those resulting from upstream enrichment or biogeochemical processes.

2. Methodology

2.1. Geographic Range

We focus on the area covered by the latitude and longitude ranges of 80°–90°N and 0°–30°E, respectively, located within the WEB region (Figure 1). This includes part of the Nansen Basin, the Gakkel Ridge and part of the Amundsen Basin. This area was selected according to the World Maritime Organization (WMO) squares 1800–1802 (0°–30°E, 80°–90°N), (https://www.nodc.noaa.gov/OC5/WOD/datawodgeo.html), in order to encompass the area covered by the N-ICE2015 expedition with RV *Lance* (Figures 1 and 2). While this expedition did not cover latitudes above 83°N, we decided to keep the whole area described above that includes the "very high" Arctic to avoid subsampling the WMO squares when searching for data. The southwestern part of the selected area is under the direct influence of the Atlantic Water Inflow (Figure 2a).

2.2. Datasets Used in This Study

We used data from the N-ICE2015 expedition (Granskog et al., 2018), the World Ocean Database (WOD), a in Atlantic Ocean (CARINA), PANGEA and the database compiled by Codispoti et al. (2013), all of which are detailed below and in Table 1. Some datasets contained overlapping data, which we removed prior to analysis.

2.2.1. N-ICE2015 Datasets

During the N-ICE2015 expedition with RV *Lance,* four drifting ice camps, referred to as Floes 1–4, were established in the southern Nansen Basin of the Arctic Ocean to collect datasets of the atmosphere-snow-ice-ocean-ecosystem interactions in a thinner Arctic sea ice regime (Granskog et al., 2018; Figures 1 and 2a and Table S1). Data from several instruments are used:

Figure 2. (a) RV Lance drifts (white lines) between January 15 and June 22, 2015 during the N-ICE2015 expedition, from the Nansen Basin and across the Yermak Plateau, with underlying topography. Start and end dates of the drifts are given for the four ice floes monitored during the N-ICE2105 expedition. The yellow arrows show the approximate main pathways of the Atlantic Water (Yermak and Svalbard pass branches; adapted from Duarte et al., 2020) (b) Vertical distribution of water masses along the N-ICE2015 drift trajectory. Water-masses are labeled by color: Atlantic water (AW), modified Atlantic water (MAW), polar surface water (PSW), warm polar surface water (PSWw), intermediate water (IW), and nordic deep water (NDW) following Rudels et al. (2000) definitions. Patches of Atlantic Water are indicated coming from either the Svalbard Branch (SB), the Yermak Branch (YB), or undetermined (UB). The vertical scale is zoomed in the upper 300 m. Overlying the water masses color scale is a contour of the mixed-layer depth (white line), the photic depth under open water (green line) and the nitracline (red dots; see 2.3). The corresponding depth (m) of the seafloor along the N-ICE2015 drift trajectory shows topographic features (black; adapted from Meyer, Sundfjord, et al., 2017, refer to text).

Table 1
PANGEA, CARINA, and Codispoti et al. (2013) Datasets

Datasets	Cruise	Dates	References
PANGEA	ARK-IV/2	15/06/1987–16/06/1987	Bauch (2002), Meincke (2002) and Rohardt (2010)
	ARK-IV/3	26/07/1987–06/08/1987	Koltermann (2004) and Thiede (2006)
	ARK-XIII/2	30/06/1997–02/08/1997	Rudels (2010) and Kattner (2011a)
	ARK-XIV/2	05/09/1998–06/09/1998	VEINS Members & Fahrbach (2011)
	ARK-XV/3	27/09/1999–01/10/1999	Schauer (2010) and VEINS Members & Schauer (2011)
	ARK-XXI/1	01/09/2005–05/09/2005	Schauer and Rohardt (2010) and Kattner (2011b)
	ARK-XXVII/3	05/08/2012–29/09/2012	Rabe et al. (2013) and Bakker (2014)
	ARK-XXIX/1	28/05/2015–19/06/2015	Nikolopoulos et al. (2016) and Dybwad et al. (2020)
	ARK-XXIX/3	21/08/2015–27/08/2015	Rabe et al. (2016) and van Ooijen et al. (2016)
	ARK-XXX/2	29/07/2016–31/07/2016	Graeve and Ludwichowski (2017) and Kanzow et al. (2017)
CARINA	–	13/08/1980–15/09/1980	NODC accession number 0113607,
	–	17/08/1991–03/10/1991	https://www.ncei.noaa.gov/data/
	–	01/05/2002–04/05/2002	oceans/ncei/ocads/metadata/0113607.html
	–	24/07/2004–31/07/2004	Anderson (2007) and CARINA Group (2009)
	–	20/05/2005–21/05/2005	Jutterström et al. (2010)
Codispoti et al. (2013)	–	11/08/1972	NODC accession number 0072133
			https://www.nodc.noaa.gov/archive/arc0034/0072133/
	–	26/06/1984–22/07/1984	Codispoti et al. (2013)
	–	02/09/1997–04/09/1997	–

Note. Sampling dates are given in the third column and consider only periods when sampling took place in the domain of our study. The listed references include links to the repositories where data can be found (Figure 1).
Abbreviation: CARINA, Carbon in Atlantic Ocean.

1. Pressure, salinity and temperature from a ship-based Sea-Bird Electronics SBE911 CTD processed to 1 m vertical average and from an on-ice based Sea-Bird Electronics SBE19+ CTD, with rosettes and associated water sampling (Dodd, Meyer, Koenig, et al., 2016). For details on the CTD operation, calibration and accuracy see Meyer, Sundfjord, et al. (2017). Due to drift problems with the salinity sensor of the on-ice CTD, only bottle salinity laboratory measurements obtained from the samples collected in the rosette and associated pressure, and temperature data were considered for this study.
2. Ammonia, nitrate, phosphate, silicic acid, particulate organic carbon (POC) and particulate organic nitrogen (PON) collected in the rosettes of the CTDs described above (Assmy et al., 2016; Dodd, Meyer, Fransson, et al., 2016).
3. Nitrate from a Satlantic ISUS V3 sensor deployed from the ice (Randelhoff, Sundfjord, et al., 2016). This nitrate sensor was deployed together with the on-ice CTD and calibrated with bottle data (for details about these data see Randelhoff and Guthrie, 2016).

Some of the references cited in (1–3) contain links to the repositories where data and details on analytical methods can be found.

2.2.2. PANGEA, CARINA, World Ocean Database, and Codispoti et al. Datasets

We downloaded 10 datasets from PANGEA, filtered by *Topic* "inorganic chemistry," *Method/Device* "CTD/rosette" and *Location* "Arctic Ocean" in the geographic range 0°–30°E 80°–90°N, collected between 1987 and 2016 (Table 1 and citations therein). We tried more recent dates but did not find more nutrient data available at the time of this study.

We also used Carbon in Atlantic Oceans (CARINA) datasets with temperature, salinity and nutrients collected from discrete samples and profile observations using CTD, bottle and other instruments, between 1980 and 2005 (Table 1 and citations therein).

We retrieved data from WOD (OSD data set, Bottle, low resolution CTD and XCTD, and plankton data, https://www.nodc.noaa.gov/cgi-bin/OC5/wod/getgeodata.pl?Depth=O&WorldOcean.x=816&World-Ocean.y=39) from World Maritime Organization (WMO) squares 1800–1802 (0°–30°E, 80°–90°N), (https://www.nodc.noaa.gov/OC5/WOD/datawodgeo.html; Figure 1), covering a large part of the twentieth century and including some results for the twenty-first century, until 2005. There are some uncertainties in this data set regarding the dates of some cruises which are not clear in the available metadata. Therefore, this data set was treated separately from the other datasets (see Section 2.3).

The Pan-Arctic database compiled by Codispoti et al. (2013) was downloaded from the NOAA website under NODC accession number 0072133 (Table 1 and citations therein).

2.3. Data Analysis

Our study focuses mainly on the following inorganic nutrients: Phosphate, nitrate, and silicic acid (hereafter referred to as silica or Si for simplicity). In some cases, instead of nitrate, only the sum of nitrate and nitrite was available. Considering that the values of the former were one order of magnitude higher than those of the latter in all datasets where both were available, we assumed that nitrate + nitrite ≈ nitrate. In the case of data collected during the Norwegian N-ICE2015 expedition (Granskog et al., 2018), which covers a larger intra-annual period, we also analyzed results for ammonium, particulate organic carbon and nitrogen (POC and PON, respectively). The particulate organic fractions were sampled only to ∼200 m depth, unlike the other variables, which were sampled from ocean surface to the seafloor. This expedition took place between January and June 2015 allowing to study winter to summer changes in nutrient profiles. The total time span of the CARINA, PANGEA, and NICE2015 datasets used in this study is from 1980 to 2016, with 6 years being the longest gap between samples, allowing a long-term (∼35 years) assessment of nutrient trends in the study region. Codispoti et al. data contains only two profiles between the surface and 200 m depth for 1972 in the study region (Figure 1). Therefore, these data were not included in the figures with all remaining datasets but were considered when analyzing the nitrate ranges and depth distributions. Older datasets available in the WOD were not considered separately to extend the time span of our analysis due to the lack of clarity for the sampling dates. Therefore, the WOD data set was used as a "whole" to compare with other datasets without any attempt to resolve temporal variability.

We analyzed the data using the thermodynamic equation of seawater 2010 (TEOS-10) and conservative temperature (CT) and absolute salinity (SA) are used throughout the text (McDougall et al., 2012). We grouped biogeochemical data according to the following water masses: Polar surface water (PSW), warm polar surface water (PSWw), AW, Modified Atlantic water (MAW), water masses that can be either AW or MAW (AW/MAW), intermediate water (IW), nordic deep water (NDW), after Rudels et al. (2000) and Meyer, Sundfjord, et al. (2017) (Figures 2b and 3 Text S1 for water mass characteristics). MAW is the result of AW cooling and mixing with polar waters as it circulates through the Arctic (Rudels et al., (2000).

We provide the following statistics for the nutrients in the various water masses: median, 25th and 75th percentiles and mean ±95% confidence limits. In some datasets nutrient data are in μmol kg^{-1} but, in the vast majority, it is in μM. Moreover, data reported in most of the bibliography cited in the paper are also in μM. Therefore, we converted results from μmol kg^{-1} to μM after calculating water density at the surface using SA and CT. We used surface density because when a conversion between μM and μmol kg^{-1} is applied it should be based on the conditions of the laboratory where measurements take place (Daniel et al., 2020). Since we could not know the sample temperature or the laboratory temperature at the time of measurement, we used CT instead. This may be the case when samples are analyzed on board right after collection. We would have to accept this error, whether converting from μmol kg^{-1} to μM or from μM to μmol kg^{-1}. However, this error is small: less than 1% within a temperature range between 0 and 25°C. The disadvantage of using μM is that when comparing samples taken at different depths, we neglect the effects of pressure on volumetric concentration. However, this does not influence our results significantly, because we are looking for temporal trends and climatology values, and we are reporting consistently all values to surface conditions. Moreover,
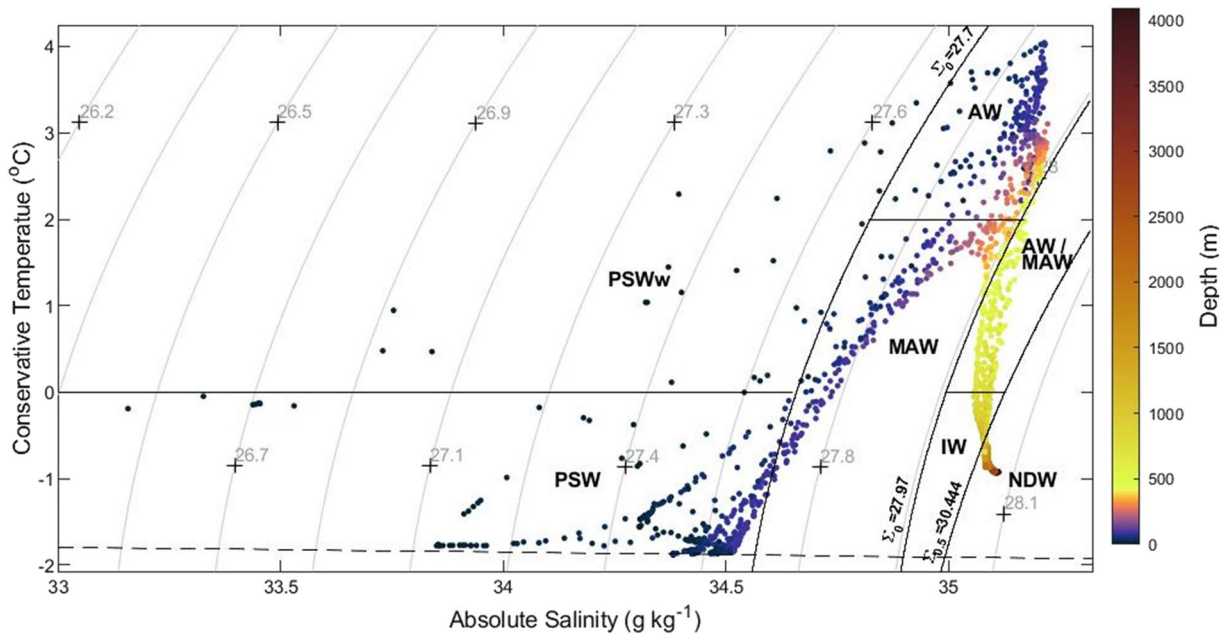
Figure 3. Conservative temperature versus Absolute Salinity from ship CTD data obtained during the N-ICE2015 expedition (see 2.2) color-coded for observation depth. Definitions of water masses following Rudels et al. (2000) are indicated: Atlantic water (AW), Modified Atlantic water (MAW), polar surface water (PSW), warm polar surface water (PSWw), Intermediate water (IW), and Nordic Deep Water (NDW). The dashed line corresponds to the freezing point of seawater.

even considering a pressure difference of 4,000 dB, the percentage change in density and the corresponding effect on volumetric concentration is less than 2%, which is not significant for the results presented in this study. Combining the error above regarding the usage of CT with this one resulting from pressure differences, we get an overall error of <2.5% in the most pessimistic scenario.

We calculated regressions between various variables and salinity to analyze their conservative behavior in different water masses. Since both variables are random, we used Model II regressions following Laws and Archie (1981). We used Model I regression to analyze temporal trends in water mass nutrient concentrations. The significance of the variance explained by the regressions was calculated by computing the ratio between explained and unexplained variance and comparing the obtained value with an F distribution at the 95% confidence level. We used One-Way ANOVA Model I with raw data and with log transformed data, and the non-parametric Kruskal-Wallis test to test differences between water masses regarding their concentrations of nitrate, phosphate and silica. Post-hoc comparisons were also used to determine significant differences between all possible pairs of water masses. The reason for the use of the Kruskal-Wallis test was the deviation from normality of the frequency distributions for nutrient concentrations in some water masses (see below) violating one of the ANOVA assumptions. This was also the reason for the use of box and whiskers plots with medians and percentiles. Despite this deviation, arithmetic means, and confidence limits are also provided in supporting information and some figures as complementary information.

Tables S2 and S3 summarize the number of samples found in the different datasets for each water mass and used in this study. The N-ICE2015 data set covers a larger intra-annual period than any other data set used in this study. Therefore, we used it to study relationships between nutrient concentrations and salinity that we later validate against data from the other available datasets.

When expressing molar ratios between nitrogen and phosphorus or nitrogen and silica, we focus on inorganic forms and use either nitrate as a proxy for inorganic nitrogen or the sum of nitrate, nitrite and ammonium, depending on data availability. When discussing the limiting role of nutrients from their concentration ratios, we focus on the limitation of biomass production yields and not instantaneous production rates.

We obtained nitrogen vertical profiles for all datasets and surface water masses. Based on the Euler method, we used these profiles to estimate a proxy of new production by integrating the area defined by the

concentration profile and the vertical line corresponding to the maximum nitrate concentration in the water mass (Figure S1). We followed the same approach of Codispoti et al. (2013), except that we did not use the differences between winter and summer profiles. We considered profiles obtained only from May onwards, covering the productive and post-productive period. Profiles were screened and only those for which we managed to detect a nitracline were further considered. We estimated the nitracline as the depth range where the nitrate depth-concentration gradient was the steepest and positive in the PSW–the dominant surface water mass (Figure 2b). We have chosen to express the obtained values in units of mass per unit of area without an explicit reference to time. This is because our data are not based on Lagrangian sampling of water masses which is the most adequate method (e.g., Moreau et al., 2020). Therefore, the time frame of the obtained results may be one or more growing seasons, depending on how fast surface water is replenished with nutrients and how fast these are consumed. If the replenishment occurs once a year, we are estimating a proxy to new production. If it occurs more or less than once a year, our results are not representative of annual new production. This will be discussed below. We used the standard Redfield ratios to convert production from nitrogen to carbon units.

Photic depth was calculated for open water using Equations 1 and 2 (Parsons et al., 1984):

$$K = 0.04 + 0.0088 \bullet \text{Chl} + 0.054 \bullet e^{2/3 \cdot \ln(\text{Chl})} \qquad (1)$$

$$Z = \frac{\ln(0.01)}{K}, \qquad (2)$$

Where K is the light extinction coefficient (m^{-1}) calculated as a function of chlorophyll concentration (Chl) in mg m^{-3} and Z is the photic depth (m) at which light intensity is 1% of surface light.

3. Results

3.1. Water Mass Nutrient Trends for the Period 1980–2016

Time series of nitrate, phosphate, and silica from 1980 to 2015 do not show any increasing or decreasing trends in the median concentrations for the various water masses (Figures 4–6). The same applies for time series with the means ±95% confidence limits (Figure S2), except in the case of silica in PSW, which showed a significant linear decreasing trend of −0.86 μM per decade. Negative trends are also apparent for nitrate and phosphate in PSW but they are not statistically significant ($p > 0.05$).

3.2. Nutrient Concentrations and Ratios in Arctic Water Masses

Nitrate, phosphate, and silica concentrations increase in water masses found deeper (Figures 2b and 7a–7c). Nitrate and, to a lesser degree, phosphate increase in a stepwise fashion, with a clear separation between the following groups of water masses: PSW and PSWw, AW and MAW, AW/MAW and IW, and NDW. Silica increases in a more gradual way and values between PSW and PSWw, on one hand, and AW and MAW, on the other hand, do not differ proportionately as much as for nitrate and phosphate. Minimal and maximal mean and median values for the different nutrients occur in PWSw and NDW, respectively (Table 2).

We observe the highest ammonium values (0.64 ± 0.30 μM) in PSWw in the N-ICE2015 data set. In all remaining water masses, ammonium values are ~0.2 μM (Figure 8a). Patterns for nitrate, phosphate, and silica in the N-ICE2015 data set (Figures 8b–8d) are like those described in the previous paragraph, when all datasets are considered, except for the smaller differences between PSW and PSWw in the N-ICE2015 data set. If we remove the N-ICE2015 data from the results shown in Figure 7, we get similar results (Figure S3). This was done to evaluate the relative importance of the N-ICE2015 data in the observed patterns given its wider intra-annual temporal range and large number of datapoints, especially for nitrate (Table S2).

Particulate organic carbon and nitrogen (POC and PON) data in the N-ICE2015 data set are available only for PSW, PSWw, AW, and MAW. POC and PON concentrations are maximal in PSWw with similar values across PSW, AW and MAW (Figures 8e and 8f).
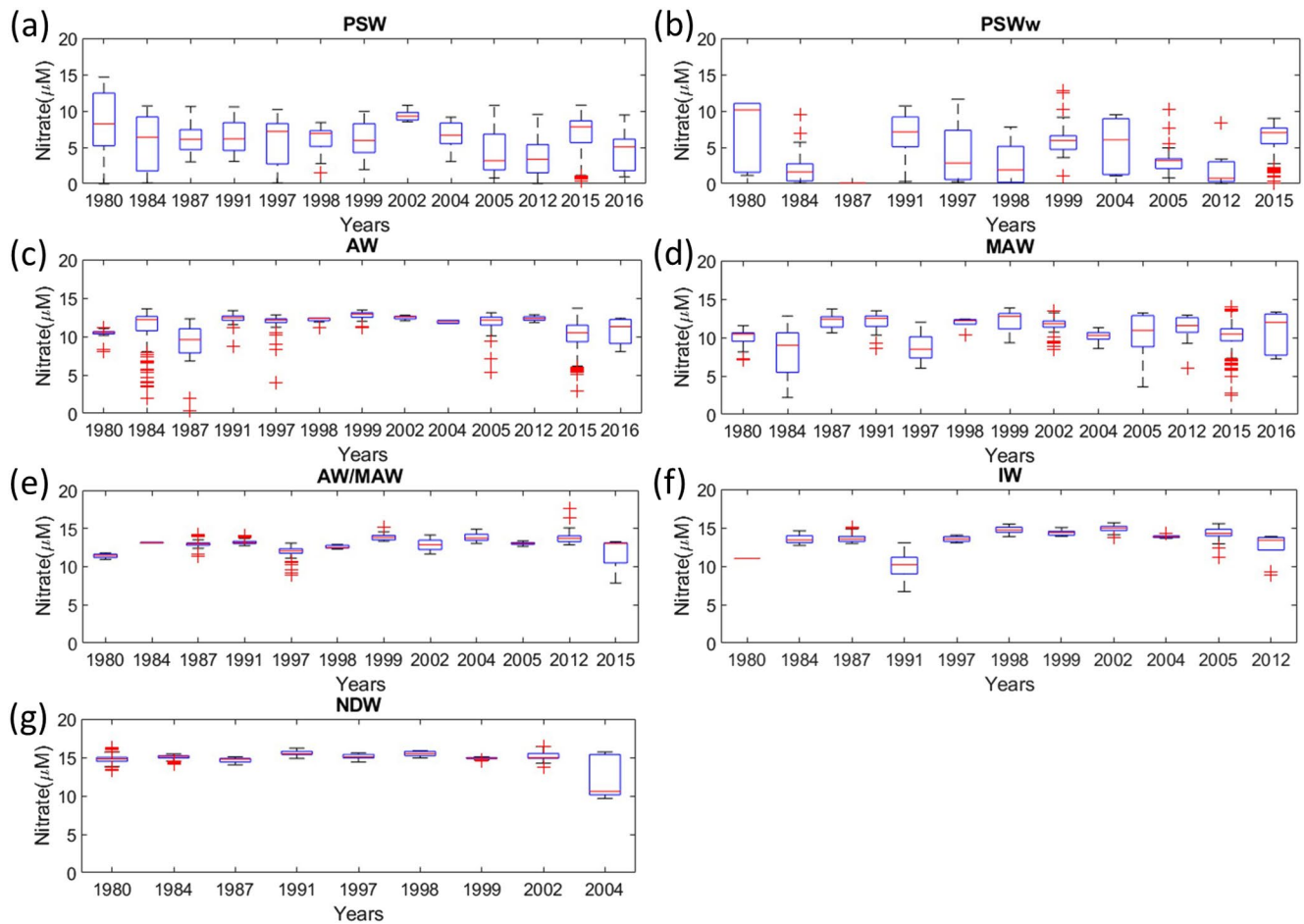
Figure 4. Box and whiskers time series plots for nitrate in polar surface water (PSW), polar surface water warmed (PSWw), Atlantic water (AW), modified Atlantic water (MAW), either AW or MAW (AW/MAW), intermediate water (IW) and nordic deep water (NDW), with data collected between 1980 and 2016 (see Methodology 2.2, Table 1 and Figure 1). Water types classified following Rudels et al. (2000) and Meyer, Sundfjord, et al. (2017). On each box, the red mark indicates the median, and the bottom and top edges of the boxes indicate the 25th and 75th percentiles, respectively. The whiskers extend to the most extreme data points not considered outliers, and the outliers are plotted individually using the "+" symbol. An outlier is a value that is, more than three scaled median absolute deviations (MAD) away from the median (see text).

We found that the medians of the molar stoichiometric nitrogen to phosphorus ratio are below the Redfield value of 16 for all water masses, whether we use nitrate as a proxy for inorganic nitrogen or the sum of nitrate, nitrite, and ammonium (DIN, when available; Figures 7d and S4a, S4b). The lowest ratios are observed in the surface water masses PSW and PSWw.

The medians of the nitrogen to silica ratios (Figure 7e) in PSW, AW, MAW, and AW/MAW are above the range generally considered representative in Arctic diatoms- between 0.96 and 1.7 (e.g., Takeda, 1998; Krause et al., 2018) -, whereas in IW and NDW, values are within that specified range. In the N-ICE2015 data set, results are similar, except for PSWw, with a nitrogen to silica ratio within the Arctic diatom range (Figure S4c and S4d). POC to PON ratios are below the expected Redfield ratio of 6.6 (Figure S4e). Their average is 5.1 across the whole water masses in the N-ICE2015 data set, with a minimum of 4.7 in PSW and a maximum of 6.7 in AW–the only value matching the expected Redfield ratio.

The frequency distributions of nitrate, phosphate and silica concentrations show deviations from normality with some being skewed toward lower concentrations, such as nitrate in PSW, PSWw, and AW, and some being skewed toward higher concentrations, such as silica in PSW and PSWw (Figures S5–S7). This skewness leads to some important differences between the means, the medians, and the modes for some water masses.
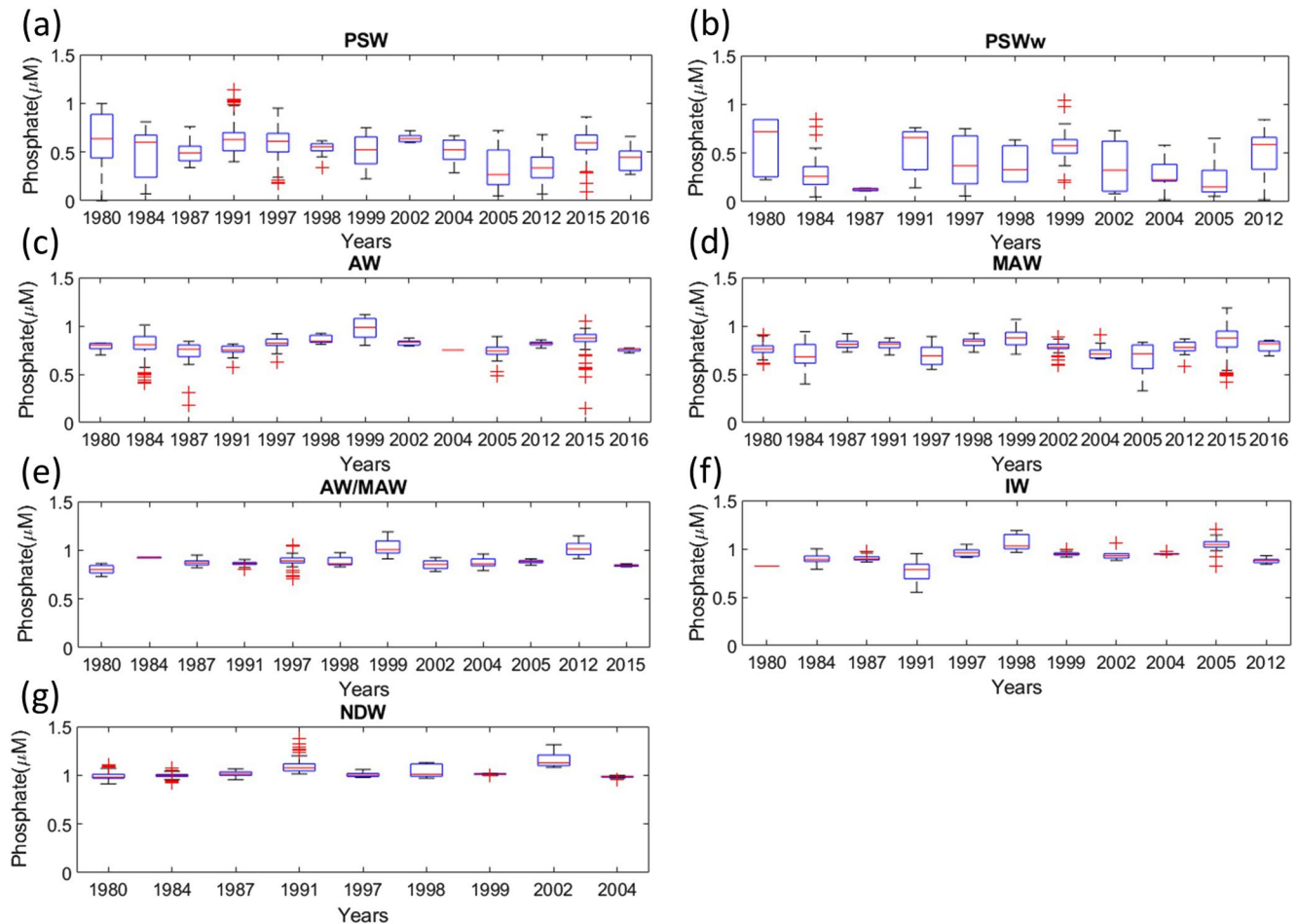
Figure 5. Box and whiskers time series plots for phosphate as in Figure 3.

ANOVA tests with raw data (Tables S4–S6), log transformed data and the Kruskal-Wallis test give consistent results leading to the rejection of the null hypothesis. Various water masses show significant differences in the concentrations of nitrate, phosphate, and silica. Post-hoc comparisons indicated that significant differences exist between almost all water masses with the following exceptions: AW versus MAW, in the case of nitrate, AW/MAW versus IW, in the case of nitrate and phosphate, and AW versus AW/MAW, in the case of silica.

We found significant relationships between salinity in PSW and the following variables in the N-ICE2015 data set: nitrate, POC, PON, nitrate to silica and nitrate to phosphate ratios (Figure 9, colored points). POC and PON (Figures 9b and 9c) decreased linearly with increasing salinity whereas the other variables increased non-linearly. Relationships between salinity in PSW and Nitrate, N:Si and N:P in other randomly selected datasets (1980 CARINA Table 1 and 2015 ARK-XXIX/1 data Table 1) are consistent with the trend lines obtained with N-ICE2015 data (Figures 9a, 9e and 9f, crosses and squares).

We also found significant positive linear relationships with salinity for nitrate, phosphate and silica, for some of the other water masses using N-ICE2015 data (Figure 10, colored points). As before, we attempted to validate some of the obtained results with other datasets selected randomly and increasing/decreasing trends with salinity were consistently observed (Figure 10, crosses, squares, and asterisks). However, despite similar trends, some datasets have significant deviations from the regression lines obtained with N-ICE2015 data, for example, for the ARK-IV/3 data (Table 1) plotted in Figures 10a and 10b as purple asterisks, where the regression lines over- or underestimate concentration values.
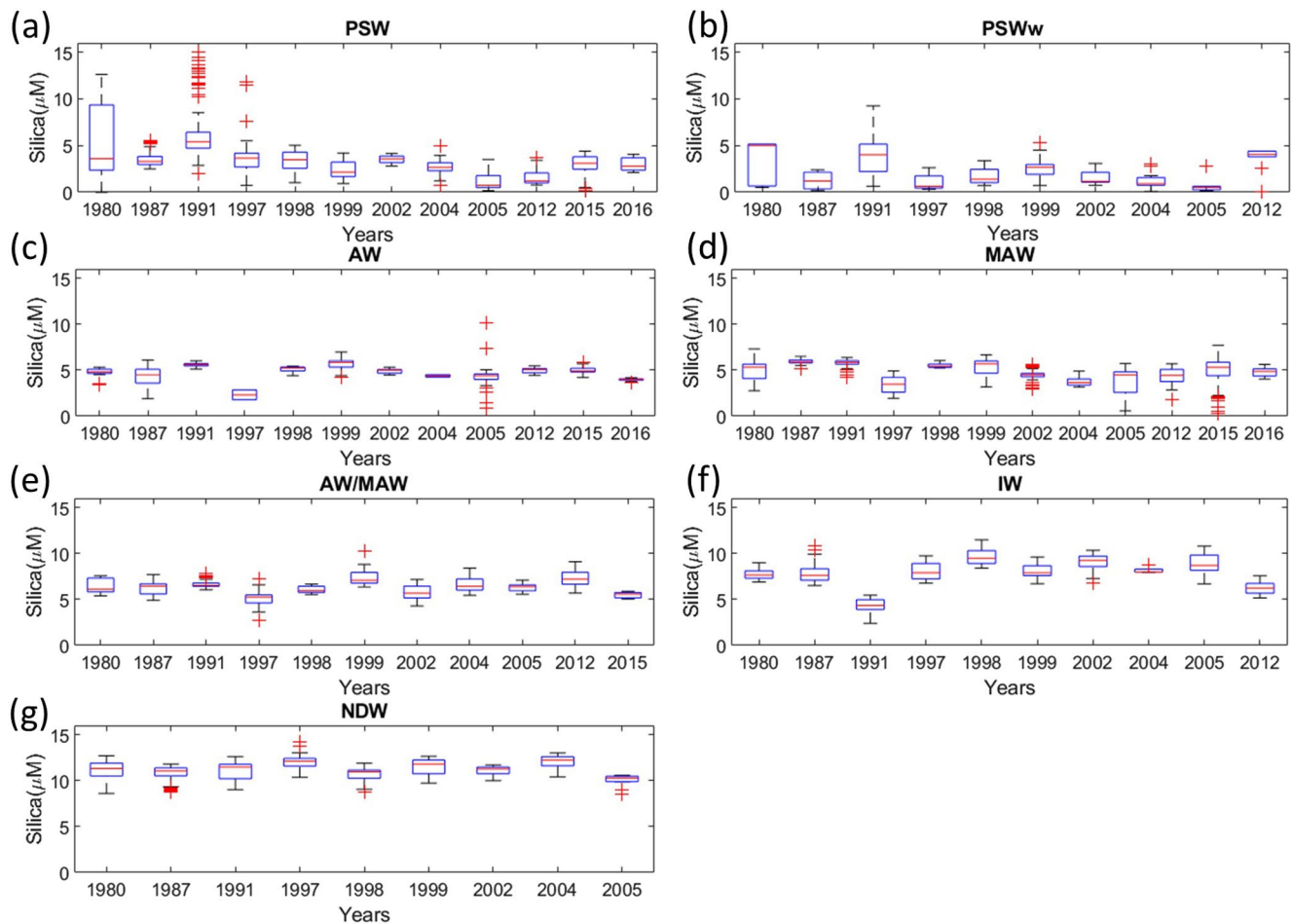
Figure 6. Box and whiskers time series plots for silica as in Figure 3.

3.3. Vertical Nutrient Profiles for the Period 1980–2016

The variability of nitrate, phosphate and silica concentrations was greatest at the surface with values from near zero to ~13, 1.2, and 15 µM, respectively. Except for some high near-surface values, concentrations increased with depth and reached their maximum values at ~1000 m, except for silica, which showed a more gradual increase with depth (Figure 11). The N-ICE2015 data set covers a larger intra-annual period (~6 months) than any of the remaining datasets (cf. Methodology 2.2 and Table 1). Its highest values for nitrate and phosphate, below ~100 m depth, are larger than those of the remaining datasets, except for the 1999 Pangea data set ARK-XV/3 (Table 1). The 2016 Pangea data set ARK-XXX/2 (Table 1 and Figures 11a and 11b) has the lowest nitrate values below ~100 m. The vertical variability and ranges of nitrate, phosphate, and silica in the N-ICE2015 data set are within the ranges of the World Ocean Database except for a few outliers for nitrate (Figures 11 and S8).

3.4. Winter to Summer Variability in 2015 Based on N-ICE2015 Datasets

Surface water masses in the Nansen Basin and the Svalbard shelf are dominated by PSW down to ~100 m over the deep ocean and ~50 m over the shelf (Figure 2b). Below the PSW there is a layer of MAW over the deep ocean and AW over the shelf and the Yermak Plateau both extending down to ~300 m. Deeper in the water column there are layers of AW/MAW, IW and NDW. Surface or near-surface patches of PSWw may be found in summer because of ice melt. Mixed layer depth ranges between ~100 m and <10 m and it is always located within the PSW layer (Figure 2b; Meyer, Sundfjord, et al., 2017). The nitracline is often shallower than the mixed layer depth, but its overall depth range is similar. The photic depth in the open ocean ranges
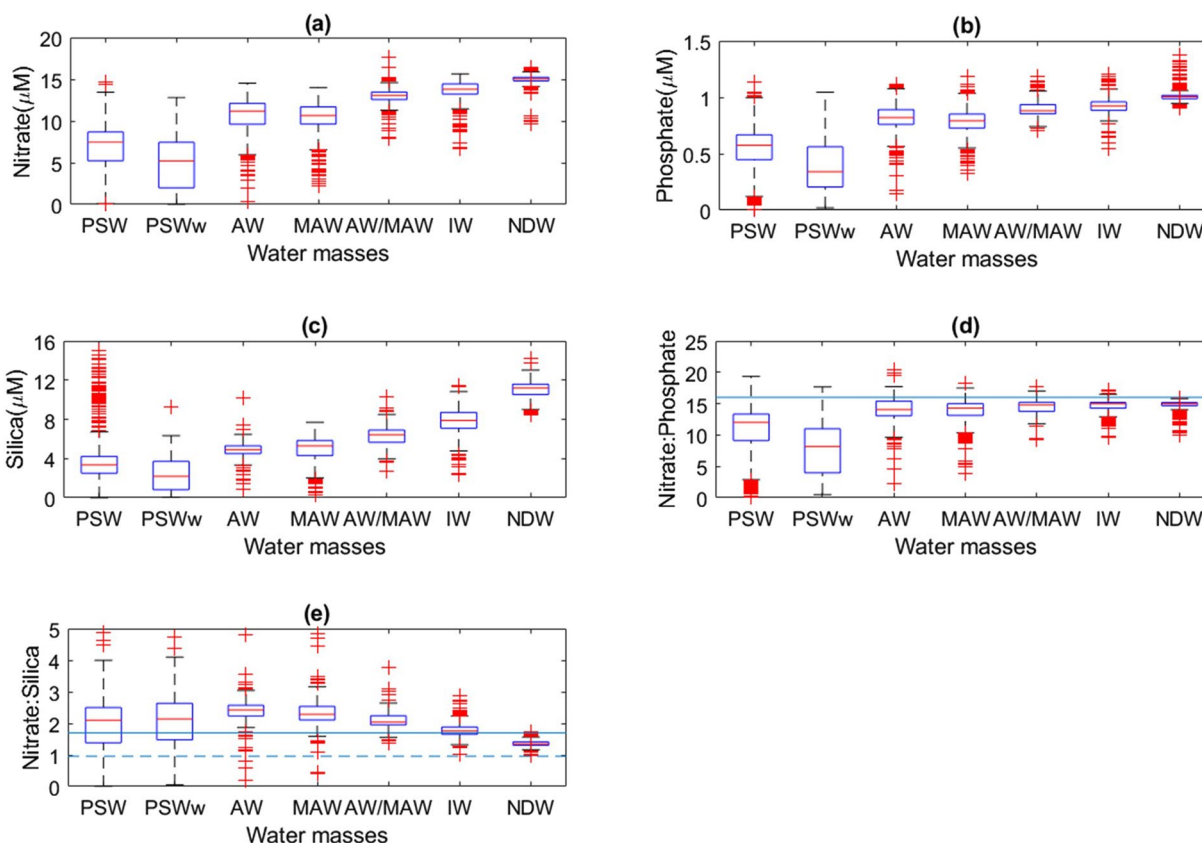
Figure 7. Box and whiskers plots for nitrate, phosphate, silica and stoichiometric molar ratios for the same water types and datasets included in Figures 3–6. The horizontal lines are the expected ratios. In the case of Nitrate: Silica two lines are given corresponding to the range reported in the literature for polar diatoms (e.g., 0.96 from Takeda, 1998, dashed line, and 1.7 from from Krause et al., 2018, continuous line; see text).

from ∼100 m to as shallow as ∼20 m (Figure 2b), during a *Phaeocystis pouchetii* dominated spring bloom, coinciding with a shallowing of the mixed layer depth, between the end of May and the end of June 2015, and described in Assmy et al. (2017).

For the N-ICE2015 data set, ammonium, silica, POC, and PON reached higher surface values between April and June (spring) than between January and March (winter; Figures 12 and S9, for a complete depth profile), whereas nitrate and phosphate exhibited opposite trends.

Table 2
Mean ±95% Confidence Limits and Median, Calculated for the Period 1980–2016 From Datasets Listed in 2.2 and Table 1, for Different Variables, in the Different Water Masses

		PSW	PSWw	AW	MAW	AW/MAW	IW	NDW
Nitrate	Mean ± CL	6.91 ± 0.10	4.83 ± 0.31	10.66 ± 0.09	10.55 ± 0.11	12.98 ± 0.12	13.56 ± 0.20	14.94 ± 0.06
	Medians	7.46	5.22	11.19	10.65	13.08	13.81	15.03
Phosphate	Mean ± CL	0.56 ± 0.01	0.38 ± 0.03	0.82 ± 0.01	0.78 ± 0.01	0.90 ± 0.01	0.93 ± 0.01	1.01 ± 0.01
	Medians	0.58	0.34	0.82	0.79	0.88	0.92	1.00
Silica	Mean ± CL	3.85 ± 0.17	2.33 ± 0.30	4.86 ± 0.10	4.94 ± 0.11	6.33 ± 0.12	7.81 ± 0.21	11.04 ± 0.10
	Medians	3.35	2.18	4.9	5.3	6.44	7.89	11.20

Abbreviations: AW, Atlantic water; IW, intermediate water; MAW, modified Atlantic water; NDW, nordic deep water; PSW, polar surface water; PSWw, polar surface water warm.
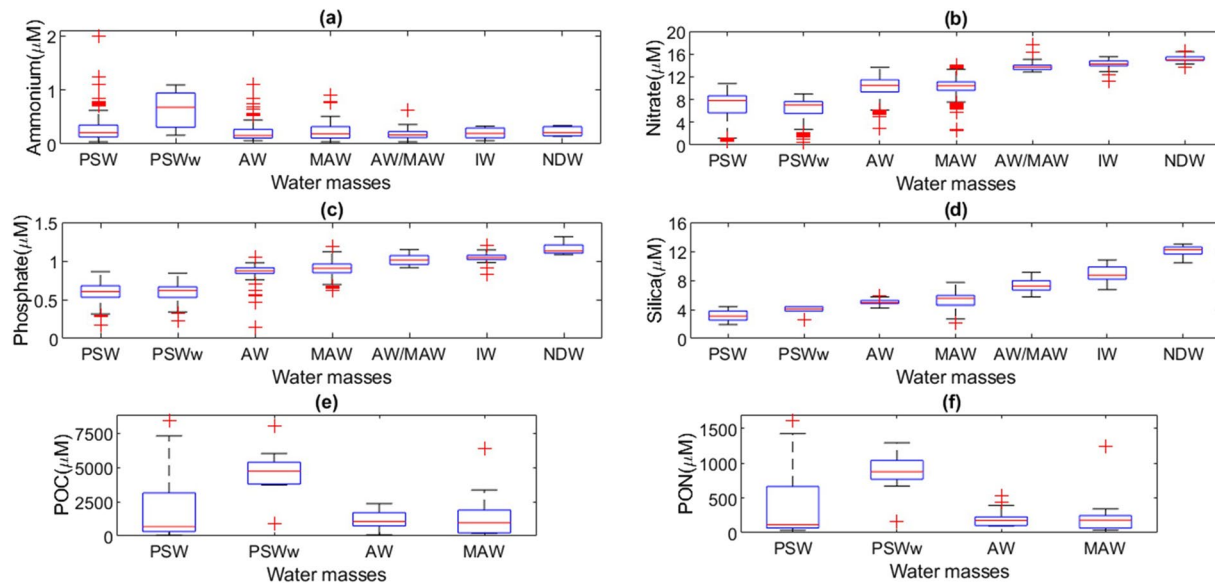
Figure 8. Box and whiskers plots for ammonium, nitrate, phosphate, silica, particulate organic carbon (POC) and particulate organic nitrogen (PON) from N-ICE2015 datasets for the same water types included in Figures 3–6 (Methodology 2.2).

3.5. New Production in Polar Surface Water

New production calculated from PSW vertical nutrient profiles ranged from 0.3 to 8.7 g N m^{-2}, corresponding to 2.0–49.4 g C m^{-2} with an average of 15.2 g C m^{-2} for the 1980–2016 period. Profiles used in these calculations are presented in the supporting information (Figures S10–S13). We did not find any significant temporal trend in the estimated new production.

4. Discussion

4.1. Long-Term Trends in Nutrient Concentrations

This analysis found no long-term trends in water mass nutrient concentrations (medians and means considered), except for a linear negative trend in the mean silica concentration in PSW. This negative trend in surface silica concentration in the study region, during the period 1980–2016, does not result from temporal changes in the sub-surface and deep-water masses, where such trends were not observed.

The absence of silica concentration trends in AW is in apparent contradiction with decreasing silica trends reported for the upper mixed layer in Atlantic Water in the Norwegian and Barents Sea (Rey, 2012), and the winter mixed layer across the subpolar Atlantic (Hátún et al., 2017). One possible explanation for this could be the use by both Rey (2012) and Hátún et al. (2017) of pre-bloom data only (March), whereas in our study we use data collected mostly in spring and summer. Winter data are extremely rare at the high latitudes covered by our study making it challenging to focus on pre-bloom data only to compare with the Rey (2012) and Hátún et al. (2017) studies. Moreover, the position of the Marginal Ice Zone after the return of light to the Arctic determines to a great extent the beginning of the bloom season and the phenology of the bloom is highly dependent on the latitude (e.g., Leu et al., 2011). Therefore, the pre-bloom season is extremely variable in our area of study. Another explanation for the differences compared to Rey (2012) and Hátún et al. (2017) findings could be the different time spans of the data (1980–2016 in our study vs 1990–2010 in Rey, 2012 and 1990–2015 in Hátún et al., 2017). If we focus on the dates covered by the two other studies, we see a slightly negative trend in silica (Figures 6c and S2c, for median and average concentrations, respectively). In order to compare in detail our results to those shown in Figure 2 of Rey (2012) and Hátún et al. (2017) we replotted the time series of silica average concentrations for AW, together with absolute salinity (Figure 13). We calculated a regression between silica concentration and date (year), after removing the lowest silica concentration of the datasets used in our study–a value for 1997 based on the only two measurements available for AW. The obtained regression, while close, is not significant considering the 95%
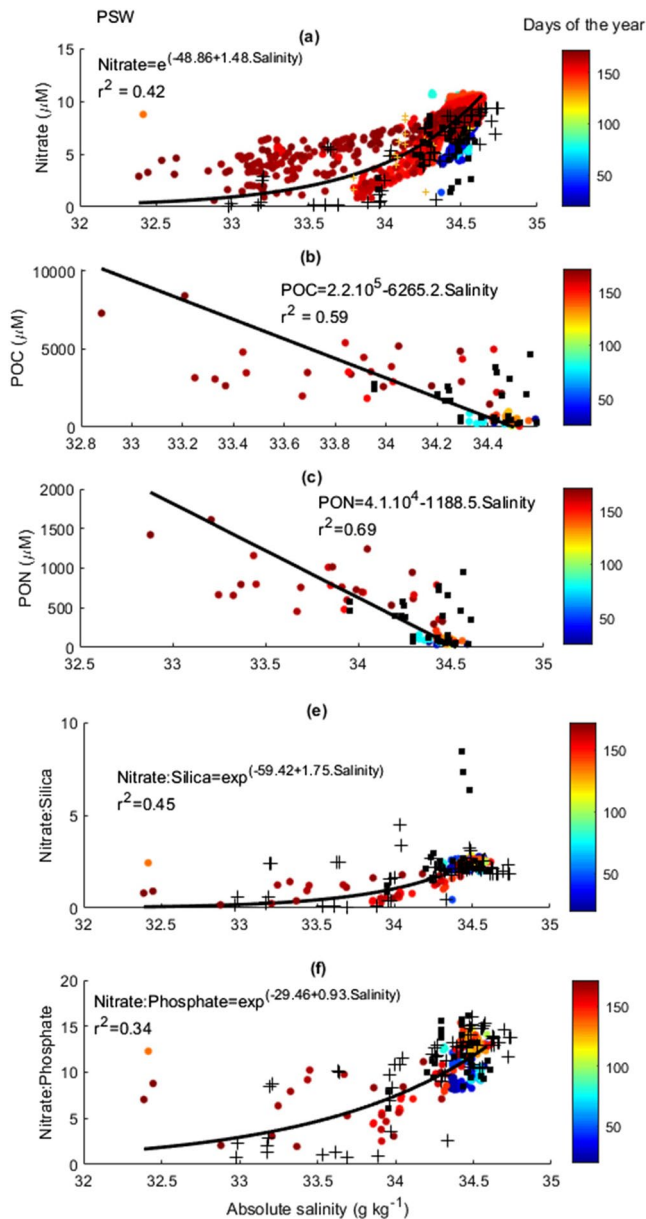
Figure 9. Nitrate, particulate organic carbon (POC), particulate organic Nitrogen (PON) and, nitrate to silica and nitrate to phosphate ratios as a function of salinity for polar surface water (PSW). Linear or non-linear significant regressions (Model II) also shown ($p < 0.05$, based on a F test between explained and unexplained variance). Regressions are based only on the colored points, corresponding to N-ICE2015 data. Colors indicate the day of the year corresponding to each observation. Black crosses in (a), (e) and (f) are 1980 carbon in Atlantic Ocean (CARINA) data (Table 1). Black squares are 2015 ARK-XXIX/1 data (Table 1).

confidence level threshold ($p < 0.07$). If we consider instead the median concentrations, we get a similar regression line with $p < 0.06$. For both regressions, the slope is ~-0.40 µM per decade–the same magnitude as estimated by Rey (2012) and Hátún et al. (2017). However, we emphasize here the absence of significant trends, even more so, when the entire silica data shown in Figure 13 are considered ($p > 0.40$), due to relatively lower values observed prior to 1990. We did not obtain any significant trends for absolute salinity, whichever period was considered.

Possible explanations for the negative silica trend in PSW are changes in nutrient inputs from land, in vertical mixing patterns or in biogeochemical processes (Polyakov et al., 2020). With the ongoing warming trends in the Arctic and expected increases in land drainage, it is unlikely that land inputs would be responsible for the decrease in silica concentrations but would rather serve as a net source. Evidence points to an increase in vertical mixing associated with the warming of AW, weakening of the halocline, and weaker stratification in the European Basin (Polyakov et al., 2020). Longer periods of reduced sea ice cover and correspondingly larger wind fetch, and the increase in the frequency and duration of winter storms (Graham et al., 2019) may further contribute to deeper ventilation, also leading to increased mixing. This increased mixing, everything else being equal, should lead to positive trends in nutrient concentrations in PSW. It can be argued that the apparent decrease in silica over the period 1990–2015 in AW (even though not significant, see above) could explain the negative trend in PSW. However, this is unlikely given the higher trends in PSW as compared with AW (~-0.84 vs. ~-0.40 µM per decade). Therefore, nutrient utilization by biogeochemical processes is the most likely explanation for decreasing silica trends in PSW. This is consistent with increasing trends in Arctic annual primary production in open waters, over the period 1998–2012 (Ardyna & Arrigo, 2020; Arrigo & van Dijken, 2015).

4.2. Nutrient Concentrations and Ratios in Arctic Water Masses

Results presented here show a relatively large range of surface values for nitrate, phosphate, and silica. Ranges at greater depths are much lower. These differences result mainly from the seasonality of primary production leading to surface nutrient depletion (lower concentrations) when phytoplankton and/or ice algal blooms take place in the spring and summer (see Assmy et al., 2017; Smith et al., 1991).

Water masses found at the surface are PSW and PSWw (Figure 2b). PSWw is typically the result of ice melt (Rudels et al., 2000). Its frequently lower nutrient concentrations in the 1980–2016 data (Figure 7), combined with higher POC and PON (observed in the N-ICE2015 data set, Figure 8), when compared to PSW, likely result from sea ice-related physical and biogeochemical processes. Sea water is the main nutrient source for ice algae biomass production (Cota & Sullivan, 1990; Cota et al., 1991). During ice growth, salt and nutrients are removed from the ice matrix through brine rejection. If there were no biogeochemical processes in the sea ice, bulk nutrient concentrations would scale with salinity, that is, decreasing exponentially with time (Turner et al., 2013 and e.g., Figure 3b in Duarte et al., 2017). When sea ice melts, algal and detrital particles may shortly increase POC and PON in waters just below the sea ice. Therefore, sea ice loses nutrients during ice growth, through brine
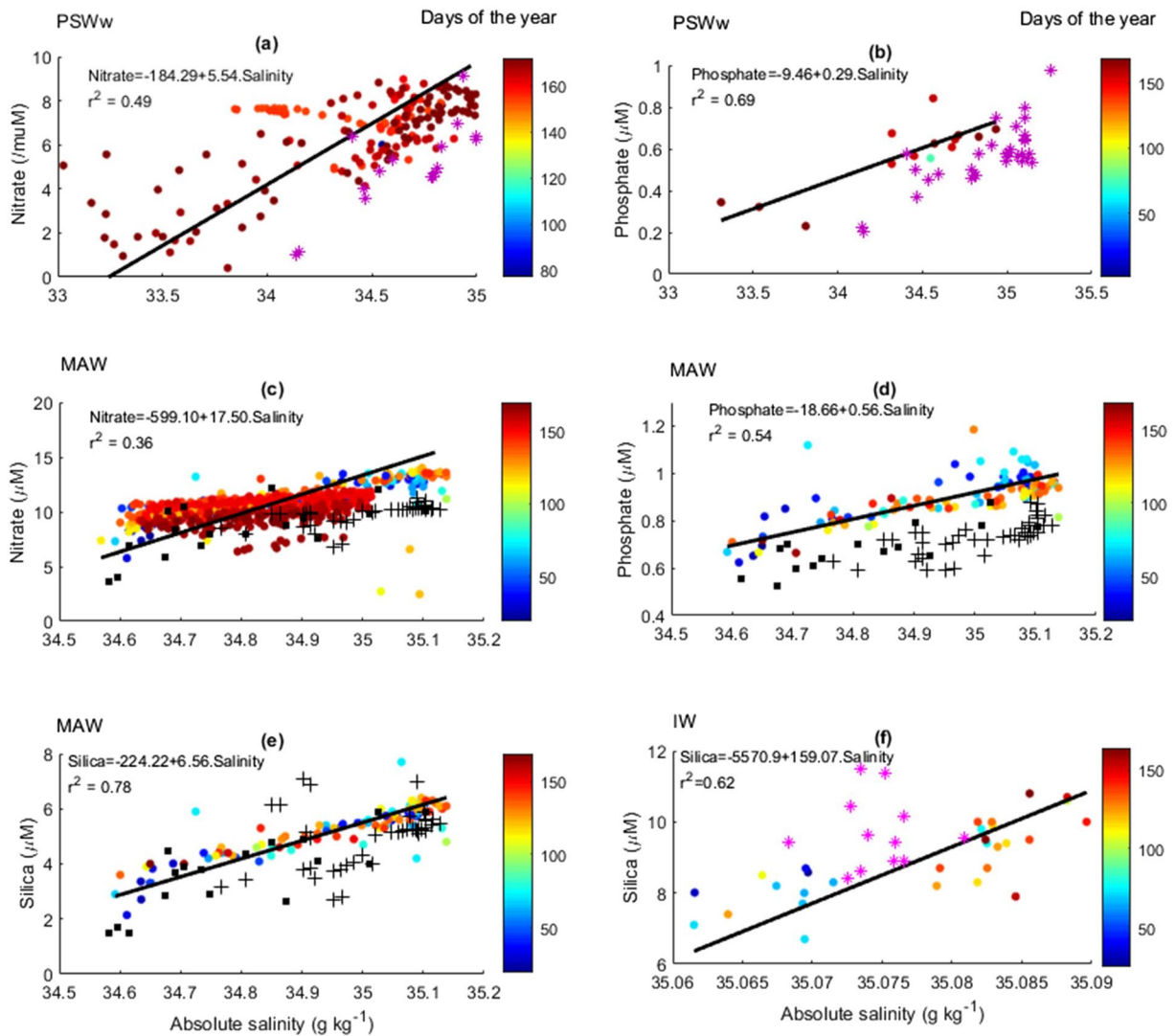
Figure 10. Plots showing linear significant regressions (Model II; $p < 0.05$, based on a F test between explained and unexplained variance) between inorganic nutrients and salinity for various water masses indicated at the upper left corner of each panel: Polar Surface Water warmed (PSWw); Modified Atlantic Water (MAW) and Intermediate Water (IW). Regressions are based only on the colored points, corresponding to N-ICE2015 data. Colors indicate the day of the year corresponding to each observation. Black crosses and squares in (a), (e) and (f) are 1980 CARINA data (Table 1) and 2015 ARK-XXIX/1 data, respectively. Purple asterisks in (a), (b) and (f) are 1987 ARK-IV/3 (Table 1).

rejection and later, during ice melt, through the sinking of particulate organic matter containing nutrients used by microorganisms and leading to a tight sympagic-benthic coupling (e.g., Boetius et al., 2013).

The relatively low N:P and high N:Si ratios in surface water masses (PSW and PSWw) show that water column primary production yields are mostly nitrogen or silica limited, in the case of diatoms. Note that we use N:P and -N: Si as a proxy to DIN:P and DIN:Si, except in the case of the N-ICE2015 data set, where DIN was computed from nitrate, nitrite and ammonia for a large number of samples. Ice algal blooms are typically dominated by diatoms (Leu et al., 2015) and it is probable that pelagic and sea ice diatoms do not use all available nitrogen, which may then be used by other non-diatom primary producers. This is consistent with the occurrence of flagellate blooms in Arctic waters (e.g., Ardyna & Arrigo, 2020; Assmy et al., 2017; Cota et al., 1994; Smith et al., 1991). Moreover, silica rather than nitrogen limitation was already suggested to be responsible for bloom termination in Atlantic Arctic and Subarctic provinces, based on a 6-weeks survey during the bloom period (Krause et al., 2019). The high N:Si ratios in surface waters (PSW and PSWw) is
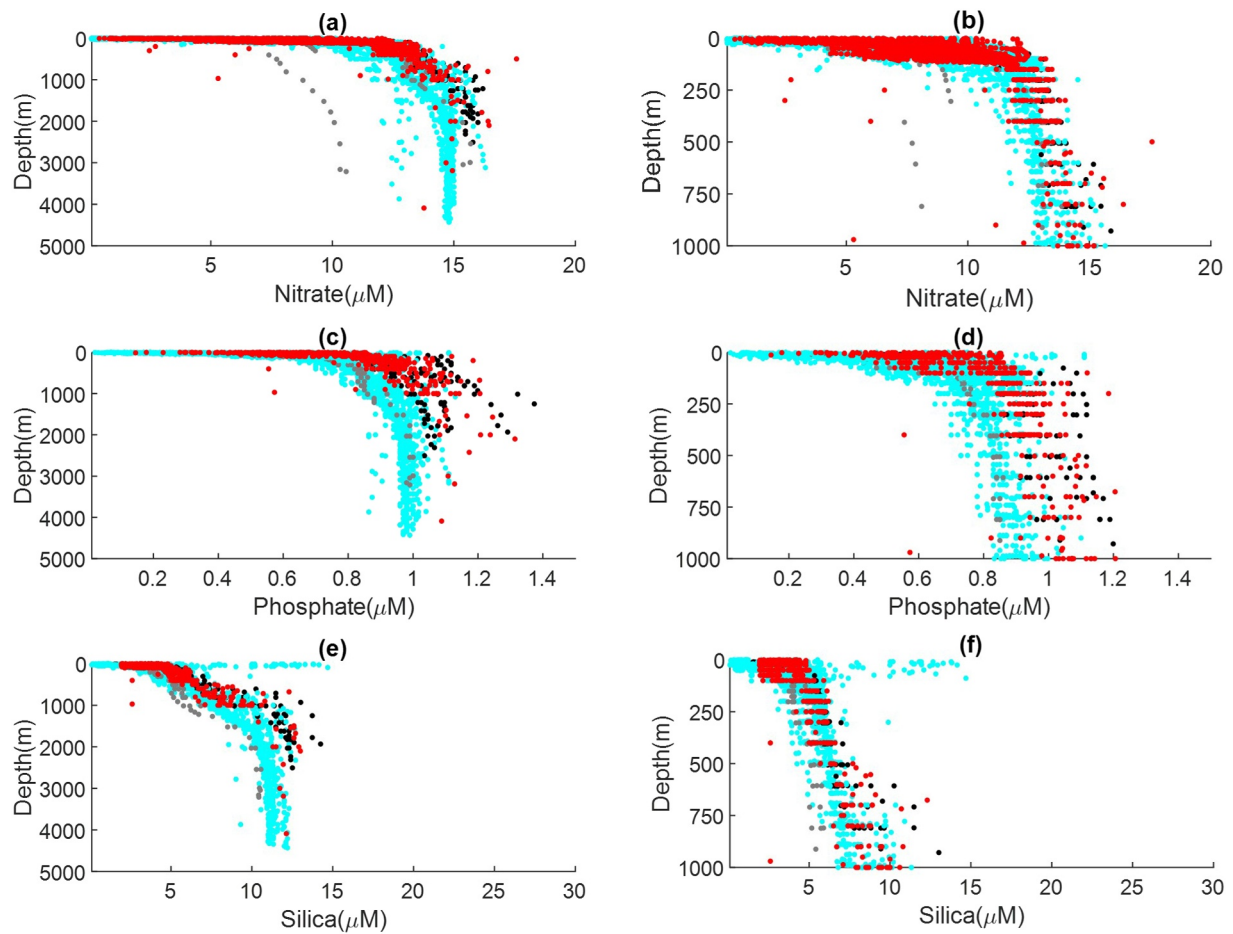
Figure 11. Vertical profiles of nitrate (a and b), phosphate (c and d) and silica (e and f) from 1999 ARK-XV/3 (black dots) and 2016 ARK-XXX/2 (gray dots), N-ICE2015 datasets (red dots) and remaining carbon in Atlantic Ocean (CARINA), PANGEA and Codispoti et al. (2013) datasets (cyan dots). Left panels show the whole depth range of available data. Right panels show only the upper 1000 m for higher vertical resolution (see text).

primarily a result of their mixing with AW and MAW, both having high N:Si values. Therefore, silica limitation is likely imprinted to the surface polar waters from their main nutrient sources–AW and MAW.

Significant relationships between nutrients and salinity are predominantly conservative for PSWw, MAW and IW, with consistent increasing trends between various datasets and showing that: (a) deeper and more saline water masses serve as nutrient sources for shallower water masses; (b) mixing and dilution may explain more than 50% of the nutrient concentration variability (e.g., r^2 values >0.5 in Figure 10 for phosphate vs. salinity in PSWw and MAW and, for silica vs. salinity in MAW and IW); (c) biogeochemical processes appear of lesser importance given the linearity of the trends. However, in the case of PSW, the exponential positive (Figures 9a, 9e and 9f) relationships of nitrate, N:Si and N: P ratios with salinity are non-conservative (non-linear) and suggest that PSW acts as a nitrate sink. The negative trends of POC and PON with salinity in PSW result from the dilution of organic matter produced near the surface.

The average POC–PON ratio (5.1) is below the expected Redfield ratio of 6.6 but well within ranges reported for the Arctic (Crawford et al., 2015 and references therein). As pointed out by Crawford et al. (2015), such results have ramifications for the conversion between carbon and nitrogen-based estimates of primary production and for biogeochemical modeling where standard Redfield ratios are frequently assumed when converting between carbon and nitrogen. Relatively low POC: PON ratios as presented here, can be associated with a large contribution of small flagellates to phytoplankton carbon (Crawford et al., 2015), which is likely the case in our domain during the N-ICE2015 expedition (Figure 2), where the only water column bloom observed was dominated by *P. pouchetii* (Assmy et al., 2017). However, our low POC: PON values
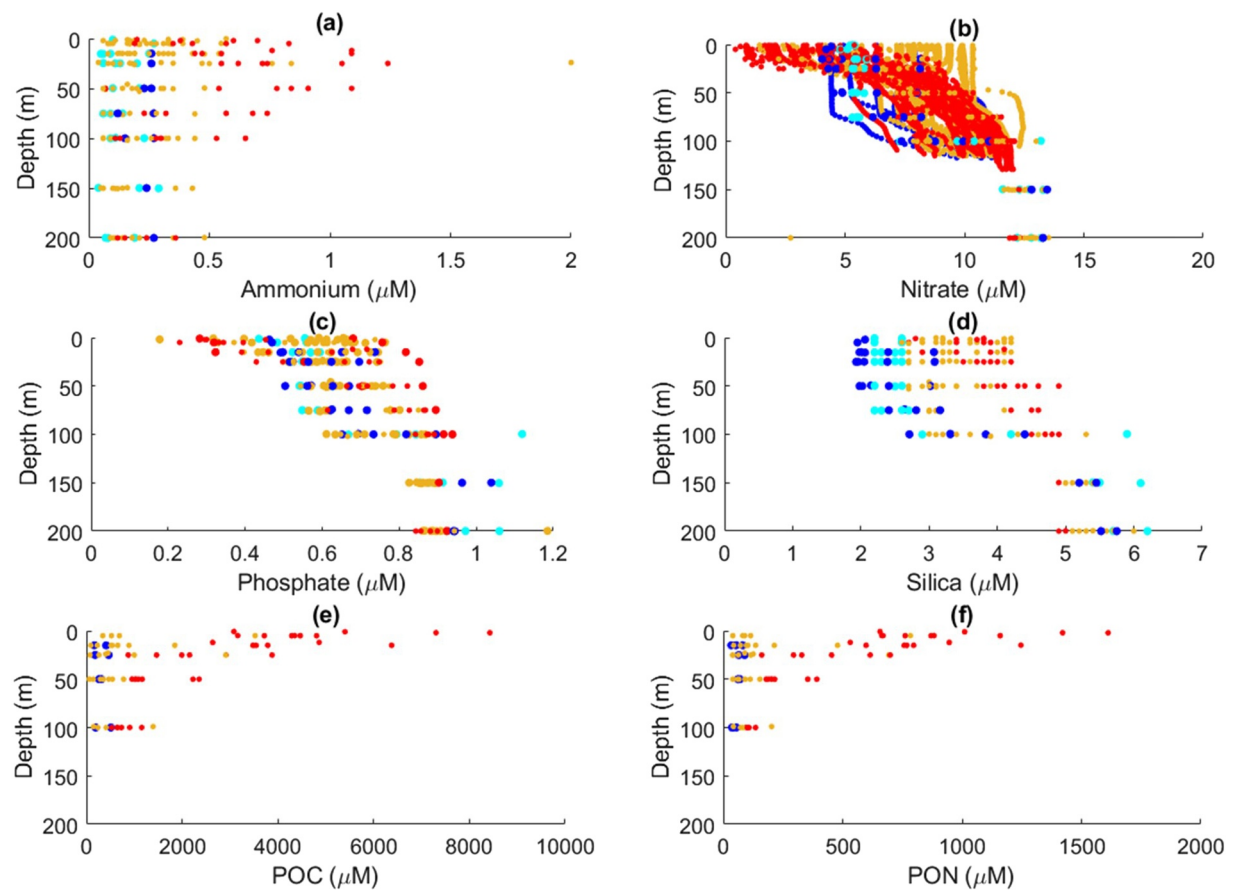
Figure 12. Plots for ammonium, nitrate, phosphate, silica, particulate organic carbon (POC) and particulate organic nitrogen (PON), from N-ICE2015 datasets (Methodology 2.2) and for the four ice floes sampled in the dates indicated next to the legend (see also Figure 2a). Only the top 200 m are shown for better vertical resolution (POC and PON were sampled solely to 100 m). The larger number of sampling points for nitrate reflects the contribution of data obtained with a nitrate sensor.

contradict results obtained in 2014 along the Atlantic Water Inflow and its Svalbard Branch, including some data collected close to the N-ICE2015 floe 2 region (Figure 2), with values always above the Redfield ratio in all seasons, within the upper 100 m (Paulsen et al., 2018).

Our results show clear differences in nutrient concentrations between the various water masses. A silica versus nitrate plot, using both the mean and the median concentrations, clearly separates all water masses except AW from MAW (Figure 14). This confirms to some extent the "natural" biogeochemical separation between the water masses.

The existence of very low nitrate concentration values in PSW is both a result of biogeochemical consumption and insufficient replenishment of PSW due to limited mixing with AW or MAW. There is a sharp decrease in the frequency histogram for values above 10 μM of nitrate in PSW (Figure S5), which likely represents an asymptotic concentration capped by mixing with AW or MAW. We may apply mass conservation principles to calculate the maximum amount of AW that may be mixed with PSW without changing its
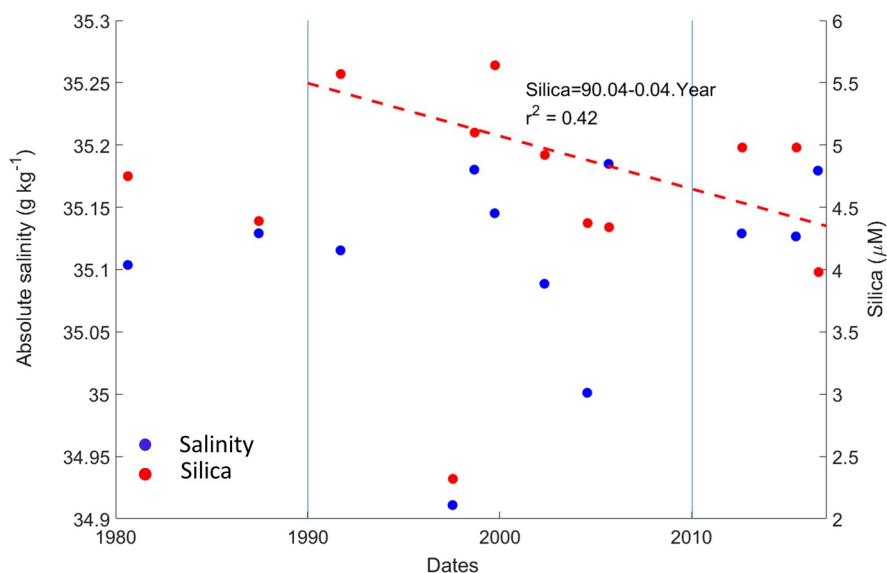
Figure 13. Time series of silica and absolute salinity averages for Atlantic water (AW) with data collected between 1980 and 2016 (see Methodology 2.2, Table 1 and Figure 1). The silica values plotted here are the same shown in Figure S2 but this figure was formatted to allow an easier comparison with Figure 2 of Rey (2012) and Hátún et al. (2017). The vertical lines depict the starting and ending dates of the results shown in Rey (2012). Hátún et al. (2017) results are from the same date (1990) but extend until 2015. The regression line shows the negative salinity trend after removal of the lowest silica value. Water types classified following Rudels et al. (2000) and Meyer, Sundfjord, et al. (2017) (see text).

salinity beyond the range of PSW and verify if such mixing explains the maximum concentrations of nitrate observed in PSW (details on how the calculations were performed are given in Text S2 and Equations S1–S6). PSW salinity ranges from 33.0 to a little over 34.5 g kg^{-1}. Assuming a given volume of PSW with a salinity of 33.0 g kg^{-1} mixing with AW with a salinity of 35 g kg^{-1}, we obtain a final salinity of 34.5 g kg^{-1} if the ratio between the volume of AW and that of PSW equals 3 (Equation S2). If the initial nitrate concentration in PSW is 1.0 μM (representing a nitrate depleted situation) and that in AW is 12.3 μM (~modal value), we obtain a final concentration of nitrate in PSW of ~9.4 μM, very close to the 10 μM cutoff value mentioned above. Similar calculations and results may be obtained by considering MAW instead. These simple calculations show why it is unlikely to find nitrate concentrations >>10 μM in PSW.
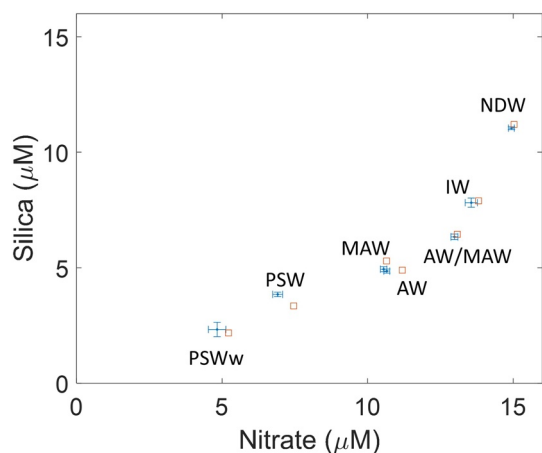

Figure 14. Silica as a function of nitrate for all water masses. Mean ±95% confidence limits (dots and lines) and medians (squares) obtained from datasets depicted in 2.2 and Table 1 for the period 1980–2016.

Randelhoff, Fer, et al. (2016) concluded that close to the shelf, upper ocean nitrate concentrations are homogeneous with depth at approximately 10 μM, from early winter until the bloom starts. According to the same authors permanent stratification exists in the deep basin, with surface mixed layer nitrate as low as approximately 5 μM. We found winter profiles matching the conclusions of Randelhoff, Fer, et al. (2016) in the N-ICE2015 datasets, but we also found profiles with high nitrate surface concentrations ~10 μM in the mixed layer over the deep basin (total depth around 3,000 m), for example, in February 13 and March 20 (Figure S10). Therefore, one may expect some spatial variability in new production based on nitrogen limitation alone, with patches of more or less N-enriched PSW.

4.3. New Production in Polar Surface Water

We may estimate a maximum for new production from the "asymptotic" nitrate concentration derived above, if PSW is the top layer. The maximum nitracline depth found in all datasets analyzed in this study was 138 m and the average was 33 m. If we consider a 138 m water column at

9.4 μM nitrate, its total removal amounts to a new production of ~1297 mmol N m^{-2} ≈ 103 g C m^{-2}, approximately twice the maximum obtained from the data analyzed in this study (49.4 g C m^{-2}).

Smith et al. (1991) calculated an average new production of 40 g C m^{-2}, from measurements of nitrate removal from surface waters during a 35-days period in the Greenland Sea in the Spring of 1989. Codispoti et al. (2013) classified the Eurasian basin as moderately productive with new production >10–~15 g C m^{-2}, over the vegetative season. Whilst the higher value reported in Smith et al. (1991) compares with the maximum of our estimates (see above), Codispoti et al. (2013) estimates compare well with our mean (15.2 g C m^{-2}) if we assume that our estimates are representative of the vegetative season (cf. Methodology 2.3).

Randelhoff, Fer, et al. (2016) compiled mixing rates across the nitracline and got average values of 0.3 and 0.7 mmol m^{-2} d^{-1} for stations with and without ice cover, respectively, and located over the Svalbard shelf, the shelf slope area, the Fram Strait and Nansen Basin west and north of Svalbard. Such values correspond to a potential carbon production of ~0.7 and 1.7 g C m^{-2} month^{-1}. If we assume a 3-months productive season, such as the "long summer period" used by Codispoti et al. (2013), those values amount to a total of ~2.1–5.1 g C m^{-2} of new production. Comparable values were estimated for the Central Arctic Ocean by Randelhoff, Fer, et al. (2016). Therefore, even when considering the larger fluxes, it would hardly be possible to match the order of magnitude of our mean estimates or those of Codispoti et al. (2013). Moreover, such mixing rates would take more than 200–500 days to replenish the PSW above the nitracline. This implies that, probably, part of the shallower PSW would take more than one year to get replenished with nitrate across the nitracline, if not for episodic intense mixing events.

Randelhoff, Fer, et al. (2016) used direct accurate estimates of dissipation rates of turbulent kinetic energy (ε) around the Svalbard shelf slope of the order ~10^{-10} −10^{-6} m^2 s^{-1} and eddy diffusivity is proportional to ε. Therefore, the nitrogen mixing rates estimated by these authors were bonded by the magnitude of ε. However, ε may be up to 10^{-5} m^2 s^{-3} during the passage of storms (Figure 2 in Meyer, Fer, et al., 2017 and Figure 4 in Peterson et al., 2017). Therefore, during storm periods of a few days, intense mixing events may take place in the water column, allowing exchanges of heat (Duarte et al., 2017) and nutrients, replenishing the PSW much faster than expected under "averaged" mixing conditions. Meyer, Fer, et al. (2017) identified the following key conditions that explain changes in the magnitude of ocean heat fluxes in the area north of Svalbard during the N-ICE2105 expedition: storms combined with the presence of shallow AW, the presence of shallow AW alone, and storms alone, in contrast to the deep Nansen Basin where storms and shallow AW were typically absent. They estimated the relative importance of each set of conditions relative to the deep Nansen Basin to follow the ratio 6:5:2:1, suggesting that the effect of storms combined with shallow AW increased ocean heat fluxes sixfold. Therefore, one may expect similar effects when it comes to mixing of nutrients. Eddies along the northern shelf of Svalbard may trap water from the slope and carry it offshore (Athanase et al., 2020) and thereafter, transport nutrient enriched waters after intense vertical mixing events, to the deep Nansen Basin.

4.4. Final Remarks

We hypothesize that:

1. the shelf region north of Svalbard with its quasi-permanent ice-free northwestern corner, known as Whalers Bay, and shallow AW (Figure 2b) is an area of large episodic heat and nutrient mixing between the AW and the PSW, where PSW is enriched with nutrients;
2. Ekman pumping (e.g., Athanase et al., 2020) brings nutrient-rich AW to shallower depths;
3. turbulent mixing reaches higher values during the passage of storms and may replenish with nutrients some patches of PSW;
4. these patches may be advected over the Nansen Basin in the form of eddies spawning from the AW boundary current, as a result of barotropic and baroclinic instabilities (e.g., Athanase et al., 2020);
5. in the deep basins and over the shelf in the absence of storms, nutrient fluxes across the nitracline are limited to low background turbulence, restricted by stratification;
6. upon release from light limitation, in open water areas or relatively transparent ice, a near-surface nitracline develops and some of the enriched patches lose their nitrogen to new production (Figure 15).
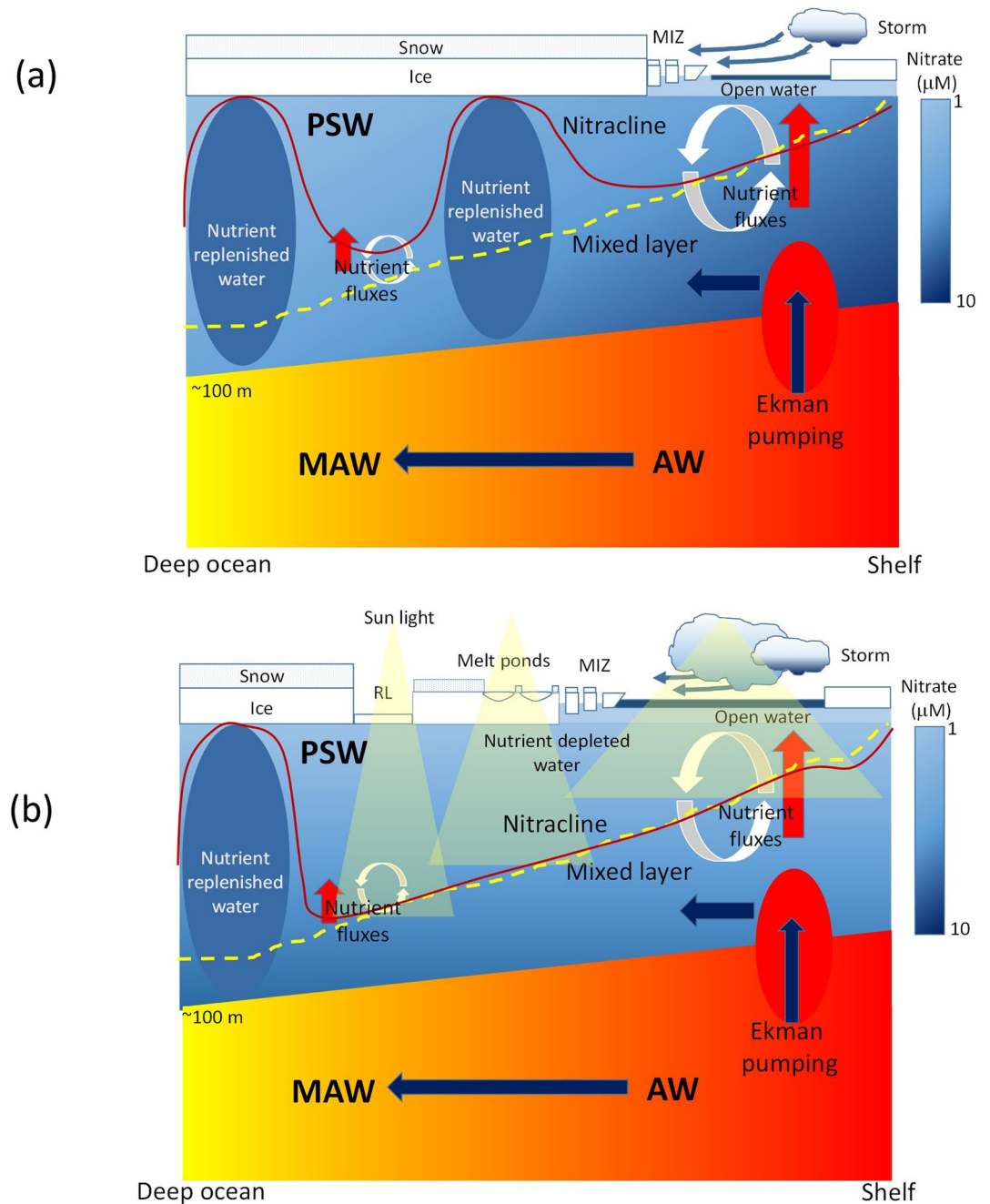
Figure 15. Conceptual model of nutrient transfer to and usage in the polar surface water (PSW). Both panels show the PSW layer and the Atlantic water (AW) or modified Atlantic water (MAW) layer, with the former predominating over the shelf (red) and the latter over the deep ocean (yellow), and a polynya over the shelf representing a place like Whalers Bay. The yellow dashed line and red line denote the mixed layer depth and the nitracline, respectively. Turbulent and convective mixing magnitude is represented by the circular arrows and red vertical arrows. Ekman pumping and isopycnical lifting is represented by the dome in AW. The blue gradient represents nitrate concentration. Patches of nitrate replenished PSW are represented as ovals. In (a) a winter situation is represented with ice and snow offshore and no sunlight. In (b) a spring-summer situation is represented with sunlight penetrating through open water and light conduits in the ice such as a refrozen lead (RL) and melt ponds. Under these spots with increased light PSW becomes nitrate depleted. Under the pack ice with thick snow cover, light limitation may prevent primary producers from using available nitrate and a replenished nitrate patch of water is represented in such conditions (see text).

5. Conclusions

In the Arctic Western Eurasian Basin, water masses may be identified based on nitrate and silica concentrations. These relatively constrained nutrient compositions, more evident in the sub-surface water masses, are useful to define boundaries for regional models as well as to evaluate model results. Nutrients scale linearly with salinity for some water masses suggesting that most of their variability is due to non-biogeochemical processes such as mixing. The exception to these is nitrate in Polar Surface Water that acts as a biogeochemical sink for nitrate. Atlantic Water has a profound influence on the Western Eurasian Basin, shaping the nutrient ratios of the Polar Surface Water. Nitrate and silica are the most likely limiting nutrients for phytoplankton and ice algal production yields, with the latter being likely more limiting than the former for diatoms, given the relatively high nitrate: silica ratios. These high ratios in Polar Surface Water result from the mixing with Atlantic Water possibly implying that diatom blooms may become silica limited before exhausting new nitrogen and, thereafter, paving the way to other non-silica dependent primary producers. We found no long-term (~36 years) changes in nutrient concentrations in the various water masses, except for a negative silica trend in Polar Surface Water, in line with the increase in primary production over the last decades reported in the literature. We hypothesize that the low background turbulent mixing rates in the Western Eurasian Basin may not be representative of the realized mixing rates, when compared to new production rates estimated from nitrate deficits. This could be explained by the Whalers Bay polynya acting as an exchange hot spot where heat and nutrients get mixed up into the mixed layer during storms, producing patches of nutrient replenished Polar Surface Water. These patches may then be advected to higher latitudes under the ice pack, either along the Atlantic Water inflow or with eddies, to later boost primary production upon release from light limitation or else, keeping a nutrient reservoir that may be used in a following vegetative season. It is rather likely that not all surface nutrients available are used every spring-summer due to light limitation under the ice pack. However, it is possible that this fraction of unused nutrients will decrease over decades to come with decreasing sea ice extent and thickness.

Data Availability Statement

The data on which this article is based are available in Bauch (2002), Meincke (2002), Koltermann (2004), Thiede (2006), Rohardt (2010), Rudels (2010), Schauer (2010), Schauer and Rohardt (2010), Kattner (2011a), Kattner (2011b), VEINS Members & Fahrbach (2011), VEINS Members & Schauer (2011), Rabe et al. (2013), Bakker (2014), Assmy et al. (2016), Dodd, Meyer, Koenig, et al. (2016), Dodd, Meyer, Fransson, et al. (2016), Nikolopoulos et al. (2016), Rabe et al. (2016), Randelhoff, Sundfjord, et al. (2016), van Ooijen et al. (2016), Graeve and Ludwichowski (2017), Kanzow et al. (2017), Dybwad et al. (2020), NODC accession number 0113607 (https://www.ncei.noaa.gov/data/oceans/ncei/ocads/metadata/0113607.html)–described in Anderson (2007), CARINA Group (2009) and, Jutterström et al. (2010) -, NODC accession number 0072133 (https://www.nodc.noaa.gov/archive/arc0034/0072133/) -described in Codispoti et al. (2013), and in the World Ocean Database (https://www.nodc.noaa.gov/cgi-bin/OC5/wod/getgeodata.pl?Depth=O&WorldOcean.x=816&WorldOcean.y=39). All these data sources are listed in the references list, except for the web sites. In the text they are cited in Table 1 and in the Methodology Section 2.2.

References

Anderson, L. (2007). *Ymer 77YM19800811 cruise data from the 1980 cruises, CARINA Data Set*. Retrieved from http://cdiac.ornl.gov/ftp/oceans/CARINA/Ymer/

Ardyna, M., & Arrigo, K. R. (2020). Phytoplankton dynamics in a changing Arctic Ocean. *Nature Climate Change*, *10*, 892–903. https://doi.org/10.1038/s41558-020-0905-y

Ardyna, M., Babin, M., Gosselin, M., Devred, E., Rainville, L., & Tremblay, J. E. (2014). Recent Arctic Ocean sea ice loss triggers novel fall phytoplankton blooms. *Geophysical Research Letters*, *41*(17), 6207–6212. https://doi.org/10.1002/2014gl061047

Arrigo, K. R., & van Dijken, G. L. (2015). Continued increases in Arctic Ocean primary production. *Progress in Oceanography*, *136*, 60–70. https://doi.org/10.1016/j.pocean.2015.05.002

Assmy, P., Duarte, P., Dujardin, J., Fernández-Méndez, M., Fransson, A., Hodgson, R., et al. (2016). *N-ICE2015 water column biogeochemistry [Data set]*. Norwegian Polar Institute. https://doi.org/10.21334/npolar.2016.3ebb7f64

Assmy, P., Fernandez-Mendez, M., Duarte, P., Meyer, A., Randelhoff, A., Mundy, C. J., et al. (2017). Leads in Arctic pack ice enable early phytoplankton blooms below snow-covered sea ice. *Scientific Reports*, *7*, 40850. https://doi.org/10.1038/Srep40850

Athanase, M., Provost, C., Pérez-Hernández, M. D., Sennéchael, N., Bertosio, C., Artana, C., et al. (2020). Atlantic water modification North of Svalbard in the mercator physical system from 2007 to 2020. *Journal of Geophysical Research: Ocean Dynamics*, *125*, e2020JC016463. https://doi.org/10.1029/2020jc016463

Bakker, K. (2014). *Nutrients measured on water bottle samples during POLARSTERN cruise ARK-XXVII/3 (IceArc) in 2012*. PANGAEA. https://doi.org/10.1594/PANGAEA.834081

Bauch, D. (2002). *Physical oceanography measured on water bottle samples during POLARSTERN cruise ARK-IV/2*. PANGAEA. https://doi.org/10.1594/PANGAEA.85209

Boetius, A., Albrecht, S., Bakker, K., Bienhold, C., Felden, J., Fernandez-Mendez, M., et al. (2013). Export of algal biomass from the melting Arctic sea ice. *Science*, *339*(6126), 1430–1432. https://doi.org/10.1126/science.1231346

CARINA Group. (2009). *Carbon in the Arctic Mediterranean seas region–the CARINA project: Results and data*. Oak Ridge National Laboratory, U.S. Department of Energy. https://doi.org/10.3334/CDIAC/otg

Codispoti, L. A., Kelly, V., Thessen, A., Matrai, P., Suttles, S., Hill, V., et al. (2013). Synthesis of primary production in the Arctic Ocean: III. Nitrate and phosphate based estimates of net community production. *Progress in Oceanography*, *110*, 126–150. https://doi.org/10.1016/j.pocean.2012.11.006

Cota, G., Legendre, L., Gosselin, M., & Ingram, R. G. (1991). Ecology of bottom ice algae: I. Environmental controls and variability. *Journal of Marine Systems*, *2*, 257–277. https://doi.org/10.1016/0924-7963(91)90036-t

Cota, G. F., Smith, W. O., Jr., & Mitchell, B. (1994). Photosynthesis of Phaeocystis in the Greenland Sea. *Limnololy and Oceanography*, *39*, 948–953. https://doi.org/10.4319/lo.1994.39.4.0948

Cota, G. F., & Sullivan, C. W. (1990). Photoadaptation, growth and production of bottom ice algae in the Antarctic. *Journal of Phycology*, *26*, 399–411. https://doi.org/10.1111/j.0022-3646.1990.00399.x

Crawford, D. W., Wyatt, S. N., Wrohan, I. A., Cefarelli, A. O., Giesbrecht, K. E., Kelly, B., & Varela, D. E. (2015). Low particulate carbon to nitrogen ratios in marine surface waters of the Arctic. *Global Biogeochemical Cycles*, *29*(12), 2021–2033. https://doi.org/10.1002/2015GB005200

Daniel, A., Laes-Huon, A., Barus, C., Beaton, A. D., Blandfort, D., Guigues, N., et al. (2020). Toward a harmonization for using in situ nutrient sensors in the marine environment. *Frontiers in Marine Science*, *6*, 773. https://doi.org/10.3389/Fmars.2019.00773

Dodd, P., Meyer, A., Fransson, A., Koenig, Z., Cooper, A., Duarte, P., et al. (2016a). *N-ICE2015 bottle data from on-ice water sampler [Data set]*. Norwegian Polar Institute. https://doi.org/10.21334/npolar.2016.089354c2

Dodd, P., Meyer, A., Koenig, Z., Cooper, A., Smedsrud, L. H., Muilwijk, M., et al. (2016b). *N-ICE2015 ship-based conductivity-temperature-depth (CTD) data [Data set]*. Norwegian Polar Institute. https://doi.org/10.21334/npolar.2017.92262a9c

Duarte, P., Meyer, A., Olsen, L. M., Kauko, H. M., Assmy, P., Rosel, A., et al. (2017). Sea ice thermohaline dynamics and biogeochemistry in the Arctic Ocean: Empirical and model results. *Journal of Geophysical Research: Biogeosciences*, *122*(7), 1632–1654. https://doi.org/10.1002/2016JG003660

Duarte, P., Sundfjord, A., Meyer, A., Hudson, S. R., Spreen, G., & Smedsrud, L. H. (2020). Warm Atlantic water explains observed sea ice melt rates north of Svalbard. *Journal of Geophysical Research: Oceans*, *125*, e2019JC015662. https://doi.org/10.1029/2019JC015662

Dybwad, C., Reigstad, M., Nikolopoulos, A., Peeken, I., & Kristiansen, S. (2020). *Concentrations of suspended and exported organic matter and nutrients during POLARSTERN cruise PS92 (ARK-XXIX/1 TRANSSIZ) in May and June 2015 north of Svalbard*. The Arctic University of Norway. https://doi.org/10.1594/PANGAEA.910883

Graeve, M., & Ludwichowski, K.-U. (2017). *Inorganic nutrients measured on water bottle samples from CTD/Large volume Water-sampler-system during POLARSTERN cruise PS100 (ARK-XXX/2)*. Alfred Wegener Institute, Helmholtz Centre for Polar and Marine Research. https://doi.org/10.1594/PANGAEA.879197

Graham, R. M., Cohen, L., Petty, A. A., Boisvert, L. N., Rinke, A., Hudson, S. R., et al. (2017). Increasing frequency and duration of Arctic winter warming events. *Geophysical Research Letters*, *44*(13), 6974–6983. https://doi.org/10.1002/2017GL073395

Graham, R. M., Itkin, P., Meyer, A., Sundfjord, A., Spreen, G., Smedsrud, L. H., et al. (2019). Winter storms accelerate the demise of sea ice in the Atlantic sector of the Arctic Ocean. *Scientific Reports*, *9*. https://doi.org/10.1038/S41598-019-45574-5

Granskog, M. A., Fer, I., Rinke, A., & Steen, H. (2018). Atmosphere-ice-ocean-ecosystem processes in a thinner Arctic sea ice regime: The Norwegian young sea ICE (N-ICE2015) expedition. *Journal of Geophysical Research: Oceans*, *123*(3), 1586–1594. https://doi.org/10.1002/2017JC013328

Hátún, H., Azetsu-Scott, K., Somavilla, R., Rey, F., Johnson, C., Mathis, M., et al. (2017). The subpolar gyre regulates silicate concentrations in the North Atlantic. *Scientific Reports*, *7*. https://doi.org/10.1038/s41598-017-14837-4.-4

Jutterström, S., Anderson, L. G., Bates, R. N., Bellerby, R., Johannessen, T., Jones, E. P., et al. (2010). Arctic Ocean data in CARINA. *Earth System Science Data*, *2*, 71–78. https://doi.org/10.5194/essd-2-71-2010

Kanzow, T., von Appen, W.-J., Schaffer, J., Köhn, E., Tsubouchi, T., Wilson, N., & Wisotzki, A. (2017). *Physical oceanography measured on water bottle samples from CTD/Large volume watersampler-system during POLARSTERN cruise PS100 (ARK-XXX/2)*. Alfred Wegener Institute, Helmholtz Centre for Polar and Marine Research. https://doi.org/10.1594/PANGAEA.871028

Kattner, G. (2011a). *Inorganic nutrients measured on water bottle samples during POLARSTERN cruise ARK-XIII/2*. PANGAEA. https://doi.org/10.1594/PANGAEA.761682

Kattner, G. (2011b). *Inorganic nutrients measured on water bottle samples during POLARSTERN cruise ARK-XXI/1*. PANGAEA. https://doi.org/10.1594/PANGAEA.761684

Koltermann, K.-P. (2004). *Nutrients measured on water bottle samples during POLARSTERN cruise ARK-IV/3*. Alfred Wegener Institute, Helmholtz Centre for Polar and Marine Research. https://doi.org/10.1594/PANGAEA.140715

Krause, J. W., Duarte, C. M., Marquez, I. A., Assmy, P., Fernández-Méndez, M., Wiedmann, I., et al. (2018). Biogenic silica production and diatom dynamics in the Svalbard region during spring. *Biogeosciences*, *15*(21), 6503–6517. https://doi.org/10.5194/bg-15-6503-2018

Krause, J. W., Schulz, I. K., Rowe, K. A., Dobbins, W., Winding, M. H. S., Sejr, M. K., et al. (2019). Silicic acid limitation drives bloom termination and potential carbon sequestration in an Arctic bloom. *Scientific Reports*, *9*. https://doi.org/10.1038/s41598-019-44587-4

Laws, E. A., & Archie, J. W. (1981). Appropriate use of regression analysis in marine biology. *Marine Biology*, *65*, 99–118. https://doi.org/10.1007/bf00397062

Leu, E., Mundy, C. J., Assmy, P., Campbell, K., Gabrielsen, T. M., Gosselin, M., et al. (2015). Arctic spring awakening–steering principles behind the phenology of vernal ice algal blooms. *Progress in Oceanography*, *139*, 151–170. https://doi.org/10.1016/j.pocean.2015.07.012

Leu, E., Soreide, J. E., Hessen, D. O., Falk-Petersen, S., & Berge, J. (2011). Consequences of changing sea-ice cover for primary and secondary producers in the European Arctic shelf seas: Timing, quantity, and quality. *Progress in Oceanography*, *90*(1–4), 18–32. https://doi.org/10.1016/j.pocean.2011.02.004

McDougall, T. J., Jackett, D. R., Millero, F. J., Pawlowicz, R., & Barker, P. M. (2012). A global algorithm for estimating absolute salinity. *Ocean Science*, *8*(6), 1123–1134. https://doi.org/10.5194/os-8-1123-2012

Meincke, J. (2002). *Hydrochemistry measured on water bottle samples during POLARSTERN cruise ARK-IV/2*. Institut für Meereskunde, Universität Hamburg. https://doi.org/10.1594/PANGAEA.84139

Meyer, A., Fer, I., Sundfjord, A., & Peterson, A. K. (2017a). Mixing rates and vertical heat fluxes north of Svalbard from Arctic winter to spring. *Journal of Geophysical Research: Oceans*, *122*(6), 4569–4586. https://doi.org/10.1002/2016JC012441

Meyer, A., Sundfjord, A., Fer, I., Provost, C., Villacieros Robineau, N., Koenig, Z., et al. (2017b). Winter to summer oceanographic observations in the Arctic Ocean north of Svalbard. *Journal of Geophysical Research: Oceans*, *122*, 6218–6237. https://doi.org/10.1002/2016JC012391

Moreau, S., Boyd, P. W., & Struttom, P. G. (2020). Remote assessment of the fate of phytoplankton in the southern Ocean sea-ice zone. *Nature Communications*, *11*, 3108. https://doi.org/10.1038/s41467-020-16931-0

Muilwijk, M., Smedsrud, L. H., Ilicak, M., & Drange, H. (2018). Atlantic water heat transport variability in the 20th century Arctic Ocean from a global ocean model and observations. *Journal of Geophysical Research: Oceans*, *123*(11), 8159–8179. https://doi.org/10.1029/2018JC014327

Nikolopoulos, A., Janout, M., Hölemann, J. A., Juhls, B., Korhonen, M., & Randelhoff, A. (2016). *Physical oceanography measured on water bottle samples during POLARSTERN cruise PS92 (ARK-XXIX/1)*. Alfred Wegener Institute, Helmholtz Centre for Polar and Marine Research, PANGAEA. https://doi.org/10.1594/PANGAEA.861866

Nishino, S., Itoh, M., Williams, W. J., & Semiletov, I. (2013). Shoaling of the nutricline with an increase in near-freezing temperature water in the Makarov Basin. *Journal of Geophysical Research: Oceans*, *118*(2), 635–649. https://doi.org/10.1029/2012jc008234

Parsons, T. R., Takahashi, M., & Hargrave, B. (1984). *Biological oceanographic processes* (3rd ed.). Pergamon Press.

Paulsen, M. L., Seuthe, L., Reigstad, M., Larsen, A., Cape, M. R., & Vernet, M. (2018). Asynchronous accumulation of organic carbon and nitrogen in the Atlantic gateway to the Arctic Ocean. *Frontiers in Marine Science*, *5*, 416. https://doi.org/10.3389/Fmars.2018.00416

Peterson, A. K., Fer, I., McPhee, M. G., & Randelhoff, A. (2017). Turbulent heat and momentum fluxes in the upper ocean under Arctic sea ice. *Journal of Geophysical Research: Oceans*, *122*(2), 1439–1456. https://doi.org/10.1002/2016JC012283

Polyakov, I. V., Alkire, M. B., Bluhm, B., Brown, K. A., Carmack, E. C., Chierici, M., et al. (2020). Borealization of the Arctic Ocean in response to anomalous advection from Sub-Arctic seas. *Frontiers in Marine Science*, *7*. https://doi.org/10.3389/fmars.2020.00491

Rabe, B., Schauer, U., Ober, S., Horn, M., Hoppmann, M., Korhonen, M., et al. (2016). *Physical oceanography measured on water bottle samples during POLARSTERN cruise PS94 (ARK-XXIX/3)*. Alfred Wegener Institute, Helmholtz Centre for Polar and Marine Research. https://doi.org/10.1594/PANGAEA.859559

Rabe, B., Wisotzki, A., Rettig, S., Somavilla Cabrillo, R., & Sander, H. (2013). *Physical oceanography measured on water bottle samples during POLARSTERN cruise ARK-XXVII/3 (IceArc)*. Alfred Wegener Institute, Helmholtz Centre for Polar and Marine Research. https://doi.org/10.1594/PANGAEA.819452

Randelhoff, A., Fer, I., Sundfjord, A., Tremblay, J.-E., & Reigstad, M. (2016). Vertical fluxes of nitrate in the seasonal nitracline of the Atlantic sector of the Arctic Ocean. *Journal of Geophysical Research: Oceans*, *121*(7), 5282–5295. https://doi.org/10.1002/2016jc011779

Randelhoff, A., & Guthrie, J. D. (2016). Regional patterns in current and future export production in the central Arctic Ocean quantified from nitrate fluxes. *Geophysical Research Letters*, *43*(16), 8600–8608. https://doi.org/10.1002/2016gl070252

Randelhoff, A., Sundfjord, A., Granskog, M. A., Meyer, A., Håvik, L., Taskjelle, T., et al. (2016). *N-ICE2015 nitrate (NO3) data from in situ profiles (ISUS V3) [Data set]*. Norwegian Polar Institute. https://doi.org/10.21334/npolar.2016.96eb41f9

Rey, F. (2012). Declining silicate concentrations in the Norwegian and Barents seas. *ICES Journal of Marine Science*, *69*(2), 208–212. https://doi.org/10.1093/icesjms/fss007

Rohardt, G. (2010). *Physical oceanography during POLARSTERN cruise ARK-IV/2*. Alfred Wegener Institute, Helmholtz Centre for Polar and Marine Research. https://doi.org/10.1594/PANGAEA.742653

Rudels, B. (2010). *Physical oceanography during POLARSTERN cruise ARK-XIII/2*. Alfred Wegener Institute, Helmholtz Centre for Polar and Marine Research. https://doi.org/10.1594/PANGAEA.742654

Rudels, B., Meyer, R., Fahrbach, E., Ivanov, B. B., Osterhus, S., Quadfasel, D., et al. (2000). Water mass distribution in Fram Strait and over the Yermak Plateau in summer 1997. *Annales Geophysicae-Atmospheres Hydrospheres and Space Sciences*, *18*(6), 687–705. https://doi.org/10.1007/s00585-000-0687-5

Schauer, U. (2010). *Physical oceanography during POLARSTERN cruise ARK-XV/3*. Alfred Wegener Institute, Helmholtz Centre for Polar and Marine Research. https://doi.org/10.1594/PANGAEA.742657

Schauer, U., & Rohardt, G. (2010). *Physical oceanography during POLARSTERN cruise ARK-XXI/1b*. Alfred Wegener Institute, Helmholtz Centre for Polar and Marine Research. https://doi.org/10.1594/PANGAEA.742621

Smith, W. O., Codispoti, L. A., Nelson, D. M., Manley, T., Buskey, E. J., Niebauer, H. J., & Cota, G. F. (1991). Importance of Phaeocystis blooms in the high-latitude ocean carbon-cycle. *Nature*, *352*(6335), 514–516. https://doi.org/10.1038/352514a010.1038/352514a0

Spielhagen, R. F., Werner, K., Sorensen, S. A., Zamelczyk, K., Kandiano, E., Budeus, G., et al. (2011). Enhanced modern heat transfer to the Arctic by warm Atlantic water. *Science*, *331*(6016), 450–453. https://doi.org/10.1126/science.1197397

Takeda, S. (1998). Influence of iron availability on nutrient consumption ratio of diatoms in oceanic waters. *Nature*, *393*(6687), 774–777. https://doi.org/10.1038/31674

Thiede, J. (2006). *Physical oceanography during POLARSTERN cruise ARK-IV/3*. PANGAEA. https://doi.org/10.1594/PANGAEA.484267

Torres-Valdes, S., Tsubouchi, T., Bacon, S., Naveira-Garabato, A. C., Sanders, R., McLaughlin, F. A., et al. (2013). Export of nutrients from the Arctic Ocean. *Journal of Geophysical Research: Oceans*, *118*(4), 1625–1644. https://doi.org/10.1002/jgrc.20063

Turner, A. K., Hunke, E. C., & Bitz, C. M. (2013). Two modes of sea-ice gravity drainage: A parameterization for large-scale modeling. *Journal of Geophysical Research: Oceans*, *118*(5), 2279–2294. https://doi.org/10.1002/jgrc.20171

vanOoijen, J. C., Rijkenberg, M. J. A., Gerringa, L. J. A., Rabe, B., & Rutgersvan der Loeff Michiel, M. (2016). *Inorganic nutrients measured on water bottle samples during POLARSTERN cruise PS94 (ARK-XXIX/3)*. Royal Netherlands Institute for Sea Research. https://doi.org/10.1594/PANGAEA.868396

Vancoppenolle, M., Bopp, L., Madec, G., Dunne, J., Ilyina, T., Halloran, P. R., & Steiner, N. (2013). Future Arctic Ocean primary productivity from CMIP5 simulations: Uncertain outcome, but consistent mechanisms. *Global Biogeochemical Cycles*, *27*(3), 605–619. https://doi.org/10.1002/gbc.20055

VEINS Members, & Fahrbach, E. (2011). *Hydrochemistry measured on water bottle samples during POLARSTERN cruise ARK-XIV/2*. Alfred Wegener Institute, Helmholtz Centre for Polar and Marine Research. https://doi.org/10.1594/PANGAEA.759130

VEINS Members, & Schauer, U. (2011). *Hydrochemistry measured on water bottle samples during POLARSTERN cruise ARK-XV/3*. Alfred Wegener Institute, Helmholtz Centre for Polar and Marine Research. https://doi.org/10.1594/PANGAEA.759131